

Article

Reproductive Success Dynamics Could Limit Precision in Close-Kin Mark–Recapture Abundance Estimation for Atlantic Goliath Grouper (*Epinephelus itajara*)

Michael D. Tringali

Fish and Wildlife Research Institute, FL Fish and Wildlife Conservation Commission, 100 Eighth Avenue S.E., Saint Petersburg, FL 33701, USA; mike.tringali@myfwc.com

Abstract: Extra-Poisson variance in annual reproductive success can affect the precision of abundance estimates made using ‘close-kin’ mark–recapture procedures. However, empirical evaluation of that variance in natural marine populations can be daunting. Here, a scaling method was used to extend a discrete-time, age-structured model, facilitating investigation of annual and lifetime reproductive success dynamics in *Epinephelus itajara*. Life tables were synthesized from fishery assessment vital rates and life history measures. For model scaling, a precise empirical estimate of effective population size for the studied population was utilized as the independent variable, and model sensitivity to an informative range of adult abundance was evaluated. The potential for sex reversal to impact reproductive success dynamics was also investigated, albeit in the absence of selective fishing pressure and potential compensatory or depensatory responses. Close-kin relationships in a genetic sample of ~300 adults collected from spawning sites in the Florida Atlantic included numerous full-sibling pairs and multi-sibling families, which is unusual for long-lived, iteroparous marine populations with broadly dispersed larvae. The highly overdispersed reproductive success dynamics modeled for this population and its atypical kinship distribution could have ramifications for planned close-kin mark–recapture analyses. The low observed effective size also has conservation implications. Both issues warrant continued genetic monitoring.

Keywords: reproductive success variance; effective population size; kinship structure; selective sweepstakes

Key Contribution: A discrete-time, age-structured model is now available for researchers to investigate annual and lifetime reproductive success dynamics in natural populations. The model requires either an independent estimate of generation effective size or annual estimates of the effective number of breeders, and a dynamic tally of abundance representative of any pre-reproductive cohort.



Citation: Tringali, M.D. Reproductive Success Dynamics Could Limit Precision in Close-Kin Mark–Recapture Abundance Estimation for Atlantic Goliath Grouper (*Epinephelus itajara*). *Fishes* **2023**, *8*, 254. <https://doi.org/10.3390/fishes8050254>

Academic Editor: Felicia C. Coleman

Received: 25 March 2023

Revised: 4 May 2023

Accepted: 6 May 2023

Published: 10 May 2023



Copyright: © 2023 by the author. Licensee MDPI, Basel, Switzerland. This article is an open access article distributed under the terms and conditions of the Creative Commons Attribution (CC BY) license (<https://creativecommons.org/licenses/by/4.0/>).

1. Introduction

Because they can now be implemented at useful scales, genetic-based capture–mark–recapture, GCMR, and close-kin mark–recapture, CKMR, are growing in popularity as tools for fishery stock assessment and other resource management. In GCMR, encounter histories and estimations of adult abundance, N_A , or total abundance, N_{A+J} , are developed directly from paired classifications of the ‘identity’ relationship, IDPs [1,2]. However, in CKMR, N_A estimation is based on parent–offspring pairs, POPs, or half-sibling pairs, HSPs, with either (or both) relationship(s) providing a proxy system for marked and recaptured individuals [3,4]. When model assumptions, including requirements regarding variance, V_k , in annual reproductive success, ARS, are satisfied, the major practical benefit of CKMR is that adequate precision is achievable with relatively sparse sampling. Quadratic gains in efficiency accompany the multiple-comparisons format. Other practical benefits of the proxy system are that the onuses of ‘tagging effects’ (e.g., mortality associated with hooking, handling, and barotrauma) and certain behavioral effects (e.g., trap-happy or

trap-shy animals) are bypassed, although individual heterogeneity in capture probabilities can arise in other ways.

The parameter V_k is a Wright–Fisher (Poisson) variance and thus ARS is considered to be overdispersed when its value exceeds the mean number of offspring, \bar{k} , produced per parent during the breeding seasons for which it is measured. Depending on the empirical circumstances, high levels of overdispersion, $\psi \gg 1$, in ARS, where $\psi = V_k/\bar{k}$, can lead to estimation bias or reduced precision in CKMR models [5]. Potential impacts depend on true population abundances, the nature of sampling, and the types of familial relationships upon which proxies are built. For example, in HSP applications, if pairs of offspring from the same year class are compared, the probability of encountering sibling matches (littermates) is expected to increase with very high levels of ψ , and corresponding estimates of adult abundance could be biased downward. For this reason, CKMR studies based on HSPs are usually designed to avoid and exclude any within-year class proxy comparisons. Although there is no directional bias in the estimate, when CKMR is based on either POPs or cross-year-class HSPs, the standard errors on N_A estimates can become elevated when ψ is very high. It is this potential loss of precision that is the concern herein.

Poisson variance in family sizes also occurs on lifetime scales, with V_k^* in lifetime reproductive success, LRS, being overdispersed when it exceeds the mean of number offspring, \bar{k}^* , produced during the reproductive lifespans, τ , of breeders in the population (i.e., $\psi^* = V_k^*/\bar{k}^* > 1$). Based on a precursor to the genetic model introduced below, it has been found that variance in LRS was somewhat overdispersed ($60 < \psi^* < 185$) for red drum (*Sciaenops ocellatus*) and southern bluefin tuna (*Thunnus maccoyii*), respectively (M. Tringali and S. Lowerre-Barbieri, unpublished data), even though their ratios of (generation) effective population size, N_e , to spawning stock abundance are quite high (i.e., $N_e/N_A > 0.1$). The annual metrics V_k and ψ have not been modeled for those species. However, for broadcast spawning marine fishes with high and indeterminate fecundity, especially those with high spawning frequencies and protracted spawning seasons [6], it is reasonable to expect that V_k will exceed \bar{k} to some degree in annual cohorts. Given the above procedural caveats for CKMR, it would seem that obtaining information regarding the magnitude of ψ and its effects on close-kin distributions should be a prerequisite for use of this method.

The Florida Fish and Wildlife Conservation Commission, FWC, is currently evaluating analytical approaches that involve non-lethal genetic sampling-and-release as means of abundance estimation for the Atlantic Goliath Grouper (*Epinephelus itajara*; [7]), hereafter, ‘goliath grouper’ (Figure 1). Goliath grouper is the largest member of the subfamily Epinephelinae in the Atlantic Ocean, reaching lengths of up to 3 m and weighing as much as 400 kg [8]. It is a long-lived, slow-growing marine fish that occupies mangrove and estuarine habitats for up to seven years before relocating as adults to nearshore and offshore reef environments [9]. Reproductive maturity reportedly occurs at ages 6–7 for females and ages 4–6 for males [10]. The oldest known goliath grouper was 37 years old [10] and was collected from waters of the Florida Gulf of Mexico. Adults tend to be solitary and territorial but aggregate to spawn during summer months [11].

As with many large-bodied reef fishes, goliath grouper populations are vulnerable to overfishing owing to relatively slow maturation, spawning aggregation behavior, a limited and increasingly degraded juvenile habitat, and high fishery desirability [12,13]. Relevant reproductive characteristics of this species are summarized in Table 1. The species was once considered to be critically endangered by the International Union for Conservation of Nature, IUCN, and is thought to be overfished throughout most of its range [14,15]. However, populations in coastal waters of the Southeastern United States have shown signs of recovery, in large part owing to an exclusive-economic-zone-wide fishing moratorium instituted in 1990 [16]. As a result, the species was downlisted to vulnerable status by the ICUN [17]. While the apparent improvement in goliath grouper populations is encouraging, more information is needed regarding spawning stock abundance. Preliminary genetic

sampling and background modeling is underway by the FWC to evaluate the application of CKMR to spawning stocks along the east and west coasts of Florida.



Figure 1. Atlantic Goliath Grouper (*Epinephelus itajara*) from the Florida Atlantic. Photo-credit: Walt Stearns, South Florida Underwater Photography Society.

Table 1. Reproductive life history traits and measures for the modeled population.

Traits and Measures	Atlantic Goliath Grouper	Reference
Age at maturity	x_{α} = 6–7 years (<i>f</i>); 4–5 years (<i>m</i>)	[10]
Longevity	x_{ω} = 37–38 years; possibly truncated	[18]
Reproductive lifespan	τ = 30–31 years (<i>f</i>); 32–33 years (<i>m</i>)	$\tau_y = x_{\omega_y} - x_{\alpha_y}$
Spawning habitat	Rocky reefs/artificial reefs/wrecks; depths of 15–50 m	[19]
Spawning season	August through mid-October	[9,11]
Spawning mode	Broadcast spawning in small groups or aggregations	[11,20–22]
Reproductive strategy	Possibly diandric protogynous	(C. Koenig, pers. comm.)
Mean batch fecundity	$\sim 50 \times 10^6$	[23]
Maximum body weight	310 kg	[12]
Maximum body length	244 cm	[12]
Female spawning frequency	unknown	–
Spawning site fidelity	84% return at 1-year interval; 78% at 2-year interval	[11]
Pelagic larval duration	30–80 d	[24]
Settlement habitat	Mangrove leaf litter	[9,18]
Juvenile habitat	Mangrove forests bordering rivers and islands	[9]

To support this evaluation, I extended a discrete-time, age-structured, deterministic model [25] with a data-informed prediction of the model’s Poisson scaling factor, ϕ , to obtain information on the mean and variance of both annual reproductive success, ARS, and lifetime reproductive success, LRS. Model initialization utilized vital rates and life

history measures obtained or synthesized from the most recent Southeast Data, Assessment, and Review (SEDAR) 47 Final Stock Assessment Report [18] and exploratory values of N_A . To predict ϕ , the model extension relied on a precise empirical genetic estimate of N_e from the Florida Atlantic goliath grouper population. This N_e estimate was based on a single-sample linkage disequilibrium analysis of multilocus genotypes derived from 33 variable microsatellite DNA loci.

Conditions and circumstances that potentially influence population vital rates (e.g., fishing mortality, compensation, and depensation) and other life history variables (e.g., sex reversal, age truncation, and early maturation) warranted attention during modeling. Because of the supposition that age classes are truncated [18], goliath grouper survival rates were modeled herein under the lowest posited scenario for maximum age, x_ω . Sex change is a common reproductive strategy among groupers [26] and there is increasing evidence (C. Koenig, pers. comm.) that goliath grouper may share a diandric protogynous strategy with the closely related giant grouper, *E. lanceolatus* [27]. Therefore, possible impacts of diandric sex change on reproductive success dynamics were quantified under varying female-to-male transition rates and patterns.

The population genetic data used to estimate N_e were also used to infer close-kin relationships directly, adopting a de novo empirical Bayes inference approach. The results for modeled reproductive success metrics were interpreted synoptically and within the context of the inferred close-kin relationships. Both analyses were used to evaluate the conformance of those metrics to CKMR assumptions and other aspects of abundance estimation for goliath grouper. The very low estimated values of N_e for the Florida Atlantic population also motivated a precautionary consideration of prospects for genetic security and reproductive resiliency in the face of erratic environmental conditions and other population stressors.

2. Materials and Methods

2.1. Model Formulation

Parameter notations used for the model are provided in Box 1.

Box 1. Parameter notations used for the hFHM. Accents for these notations are described in the text.

N_x	Number of individuals of age x alive at a given time
N_A	Number of potential adult breeders in a population
N_{A+J}	Total number of individuals (adults and juveniles) in a population
T	Length of a generation in years (see definition in text)
N_e	Generation effective population size (for age-structured populations)
N_b	Effective number of breeders producing a single-year class
\bar{k}^*	Mean lifetime reproductive success of breeders during a generation
V_k^*	Lifetime variance in reproductive success among breeders in a population
\bar{k}	Mean reproductive success of breeders in one time period (e.g., annually)
V_k	Variance in the number of newborns produced by all breeders in one time period (e.g., annually)
$b_{x,y}$	Mean fecundities at age x and sex y ; $b_{x,y}$ is scaled to constant N_{A+J} , with the quantity becoming $\hat{b}_{x,y}$
$B_{x,y}$	Mean number of newborn births produced by breeders of age x and sex y
$s_{x,y}$	Probability of survival from age x to age $x + 1$ for sex y
$l_{x,y}$	Cumulative survival through age x and sex y , where $l_1 = 1$ and $l_{x,y} = l_{x,y-1}s_{x,y-1}$ for $x > 1$
x_α	Age at maturity
x_ω	Maximum age
$\phi_{x,y}$	Poisson scaling parameter for birth rate at age x and sex y in a given time period; $\phi_{x,y} = V_{k,x,y}/B_{x,y}$
ψ	Dispersion parameter for annual reproductive success; $\psi = V_k/\bar{k}$
ψ^*	Dispersion parameter for lifetime reproductive success; $\psi^* = V_k^*/\bar{k}^*$

For diploid organisms with overlapping generations, \bar{k}^* should roughly equate to $\bar{k}^* \approx 2$ when per capita births equal deaths in the population over the timescale of a few generations. Reproduction is considered to be successful when parents produce offspring that survive to reproductive age [28]. Ignoring second-order terms and assuming equality

in male and female dynamics, the generation effective sizes, N_e , of such populations can be quantified by Hill’s [29] equation as follows:

$$N_e \approx 2\bar{k}^* N_\eta T / [V_k^* + 2] \tag{1}$$

where N_η is the number of newborn individuals in a given year class η , T is the length of the generation time, and V_k^* is the variance in LRS that applies to the newborn cohorts (new year classes). This formula, although given by Hill in terms of family size variance, also applies as an inbreeding effective size in random mating populations of a constant size [30].

Using the standard discrete-generation formula for inbreeding effective size [31], the effective number of breeders, N_b , for a given year class is as follows:

$$N_b = [\bar{k}N_A - 2] / [\bar{k} - 1 + V_k/\bar{k}] \tag{2}$$

remembering that \bar{k} and V_k are the mean and variance, respectively, in the number of newborns produced by all potential male and female breeders in one time period (herein, annually) that survive to reproductive age. Separating the variance into male and female components yields the following:

$$N_b = 4 / \left[\left[V_{k,f} + \bar{k}_f (\bar{k}_f - 1) / \bar{k}_f (\bar{k}_f N_{A,f} - 1) \right] + \left[V_{k,m} + \bar{k}_m (\bar{k}_m - 1) / \bar{k}_m (\bar{k}_m N_{A,m} - 1) \right] \right] \tag{3}$$

where f and m subscripts denote female and male contributions, respectively. As a point of interest, the left and right bracketed terms in the denominator in Equation (3) represent sampling probabilities for shared maternity and paternity, respectively, for any pair of randomly selected offspring in the cohort. Expressions for estimating effective number of breeders can also be derived in terms of the sampling probabilities for HSPs and full sibling pairs, FSPs [5,32].

In a very useful innovation, Waples et al. [25] integrated Hill’s [33] and Crow and Denniston’s [31] statistical formulations with a demographically oriented approach advanced by Felsenstein [34]. Their hybrid Felsenstein–Hill model, hFHM, which adopts properties of the well-known Leslie matrix [35], can be applied to gonochoristic or sex-changing organisms, and does not assume equality in male and female dynamics. Breeders of age x and sex y produce an average of $B_{x,y}$ offspring that survive to age $x + 1$ with an annual probability $s_{x,y}$ or perish. Waples et al. [25] defined the age-/sex-specific Poisson scaling factor $\phi_{x,y}$ as the ratio of the variance to the mean reproductive success in one spawning season (i.e., annually) for breeders of a given age and sex ($\phi_{x,y} = V_{x,y} / B_{x,y}$). In essence, $\phi_{x,y}$ quantifies the magnitude of ‘within-age’ effects for a given sex. When Poisson expectations for reproductive success of same-age same-sex breeders are random, each age and sex can be viewed as a mini-Wright–Fisher ideal population, such that $\phi_{x,y} \approx 1$ and values of $\phi_{x,y} > 1$ represent the degrees to which annual variance in reproductive success is overdispersed relative to respective mean birth rates.

As in Hill’s equation, the hybrid model assumes dynamic stability in age structure and population size over several generation intervals as well as independent probabilities of survival and reproduction [33]. Geographic closure is assumed for population dynamics (i.e., no appreciable effect on birth and death rates owing to immigration or emigration in the modeled demographic unit); see Waples and England [36] and Ryman et al. [37], for additional considerations.

With life table input and an independent estimate of N_e , sex-specific measures of the reproductive success metrics \bar{k}^* , V_k^* , N_b , \bar{k} , and V_k can be obtained from the hFHM through a novel use of the program *AgeNe* ([25]; Ecological Archives E092-126-S1). For a given life table, *AgeNe* evaluates the above parameters using a three-step sum of squares approach. Initial model conditions are set with requisite user input for age-specific (proportional) sex ratio, $SR_{x,y}$, and values of x_{ω_y} , N_1 , and $\phi_{x,y}$ (here, the demographic clock is set by defining N_h as the number of fertilized gametes (hatched eggs) that enter the system as a discrete annual cohort and N_1 as the number of ‘newborn’ offspring in their first year of life, which,

in fishery terms, would be analogous to the number of young-of-the-year fish (traditionally, fishery biologists define young-of-the-year cohorts as age-0 or age-0+; linking ages thus represents a practicality, as *AgeNe* does not accept sub-one values as input for age)). For the parameter N_{η} , it has been pointed out [6,38] that any year class from age-one, x_1 , to age-at-maturity, x_{α_y} , can be adopted to evaluate the sensitivities of model parameters to changes in N_e/N_A and N_b/N_A . Likewise, the model calibrated value of $\phi_{x,y}$ is not affected by this cohort choice. Thus, for convenience, I evaluated parameter values of interest at N_1 .

Values of N_1 will usually be unknown, as is the case for the studied population, but can be estimated from a partial life table ($s_{x,y}$, x_{α_y} , x_{ω_y} , and $SR_{x,y}$) when either an empirical estimate of N_A is available or a plausible exploratory range of N_A is specified. Investigators might have empirical knowledge of that range from fishery acoustic surveys [39], physical tagging [40], or GCMR/CKMR [2,3]. Lacking such information for goliath grouper, values of N_1 were tallied in a partial life table given initial exploratory values for N_A (see Supplementary File S1) and used as input for various model constructions.

For simplicity, I assumed that the scaling factor $\phi_{x,y}$ was constant over all ages and between sexes; subscripts in that case were dropped. Not surprisingly, true values of ϕ , while critical to the modeling and investigation of reproductive success dynamics, are rarely known for iteroparous marine fish populations. Therefore, I developed a method to predict ϕ through an extension of the hFHM and by relying on a generally available data source—population genotype data. To distinguish it from the standard model, the predictive model is denoted as scFHM. With functionality rooted in the hFHM, the scFHM has flexibility to accommodate constant or variable values for age- or sex-specific survival, age- or sex-specific fecundity, and age-specific sex ratio. During prediction, empirical estimates of N_e or N_b , when available, can be used as independent variables to solve model-generated functions for $\vec{\phi}$. For this purpose, a precise empirical estimate of N_e was obtained from population genotypes, as described below.

For the scFHM, tallied values of \vec{N}_1 along with requisite life table information were first used to initialize the hFHM. A series of calibration points were evaluated in separate model runs for a given set of conditions to generate paired data—i.e., $\{\vec{N}_e \text{ at } \vec{\phi}\}$ —for use in prediction. Best-fit predictive functions were obtained via logistic regression. For curve fitting, a minimization process was used to identify a single curve that best described the data—i.e., parameter values of the curve were adjusted until the lowest possible residual sum of square error was observed. Goodness-of-fit for linear regressions was assessed via F-statistics and R^2 values. Predicted values, $\vec{\phi}$, from resultant functions were then carried back into the hFHM to scale final estimates of \hat{V}_k , \hat{k} , \hat{N}_B , and \hat{V}_k^* . It is noted that, when empirical estimates of \hat{N}_B are available instead of \vec{N}_e , $\{\hat{N}_B \text{ at } \vec{\phi}\}$ can be calibrated instead to infer \hat{V}_k , \hat{k} , \hat{N}_e , and \hat{V}_k^* . The entire process is summarized in Figure 2.

2.2. Tissue Collections

Study tissues from Florida Atlantic specimens were procured from colleagues at the Florida State University, FSU, Coastal Marine Laboratory. Tissue collections occurred during 2011 to 2013 within Florida Atlantic coastal waters (Figure 3) and consisted of fin clips and fin rays. Tissues were stored in 95% ethanol until processing. Fish were aged by FSU biologists using sampled fin-rays and methods described in Murie et al. [41]. Fish sizes, ages, collection dates, and GPS collection coordinates were available for most specimens; primary collection data appear in Table S2 of Supplementary File S2.

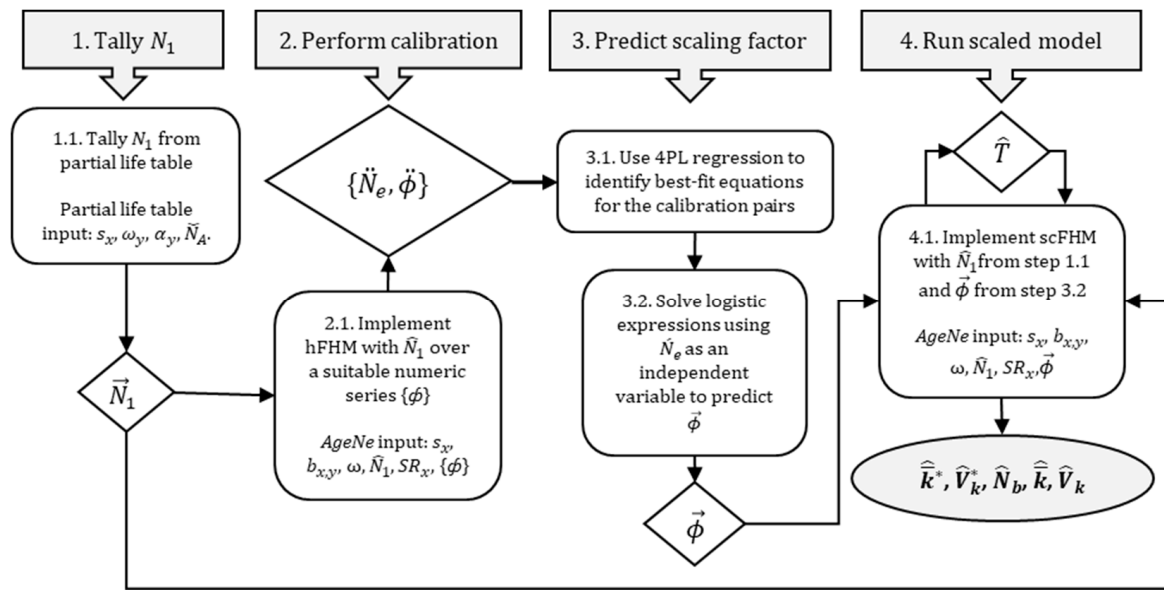


Figure 2. Summarized scFHM workflow to estimate reproductive success metrics (grey oval) when empirical estimates or exploratory ranges of spawning stock abundance (\hat{N}_A) and effective population size (\hat{N}_e) are available.

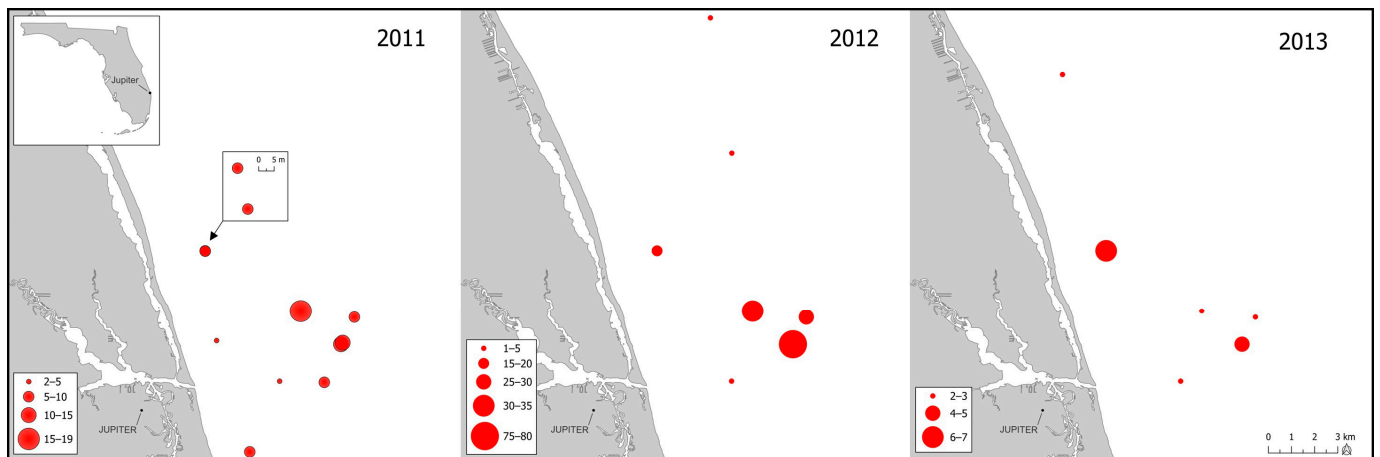


Figure 3. Locations of sampling events off the Florida Atlantic coast for *Epinephelus itajara*. Sizes of site markers reflect the numbers of specimens collected during the event (annual scales differ). Sampling was concentrated during spawning seasons at known spawning sites. Ten opportunistically sampled specimens from the Florida Keys are not shown.

2.3. Genealogical Inference

Population genotype data were based on fragment-size analyses of 36 microsatellite DNA markers. Molecular procedures, including marker description, laboratory quality assurance, and quality control protocols, and standard diversity analyses are described in Supplementary File S2. Because classification of close kin involved multiple paired comparisons of categorical relationships, \mathcal{R} , from a natural population of unknown abundance and for which sampling probabilities (i.e., priors) of the categorical relationships of interest were unknown, I developed a de novo empirical Bayes inference model for the task. The flexible approach allowed paired evaluation of all genotypes over a heuristically valid ensemble of $r = 9$ plausible categorical relationships (Appendix A). Given the sufficiency in cumulative likelihoods from the locus number and allele polymorphism (Appendix B), the sampling priors of these nine relationships can be reasonably approximated from the population genotype data via an optimization algorithm and employed as mixing weights

to greatly improve the classification accuracy (Appendix C). With a Bayes maximum a posteriori (MAP) classifier (Appendix D) and a base model calibrated with reasonably accurate mixing weights, marginal posterior expectations yield reliable predictive distributions and belief measures.

It must be noted that genotypes from independently segregating genetic loci cannot distinguish half-sibling relationships from those of avuncular and grandparent–grandchild; therefore, the acronym is hereafter denoted as HSP⁺.

2.4. Empirical Estimation of Effective Population Size

The single-sample linkage disequilibrium, LD, analysis option in *NeEstimator* V2.1 [42] was used to generate raw estimates of generation effective population size, \tilde{N}_e , for the sampled population. Estimates were formulated from the squared correlation of alleles at independently segregating gene loci [43,44]. LD analysis is based on the principle that, in closed finite populations in approximate drift–mutation–recombination equilibrium, associations between alleles among selectively neutral gene loci are a function of the generation of an effective population size. For this analysis, the moment-based genetic index is Equation (4) [43,44]:

$$E(r^2) \approx \frac{1}{3N_e} + \frac{1}{n_g} \quad (4)$$

Rewriting Equation (4) and including the sampling bias adjustment of Waples [45], \tilde{N}_e was obtained in *NeEstimator* from expected levels of allele association across loci, r^2 , as follows:

$$\tilde{N}_e = 1 / \left(3 \left(r^2 - 1/n_g \right) \right) \quad (5)$$

Because n_g varies among loci, its harmonic mean was used in Equation (5). Missing data were tabulated for each run and potential effects of low-frequency alleles on estimates were mitigated by adopting a nominal type I error rate (P_{crit}) value of 0.01 [44]. Parametric 95% and pseudo-jackknife confidence intervals [46] were recorded for all runs. Finally, raw estimates from *NeEstimator* were adjusted in silico using correction factors for physical linkage among loci [47] and mixed-age sampling [48], as described in Supplementary File S2, yielding a bias-adjusted estimate of \hat{N}_e for modeling and conservation assessment.

Waples [49] described a systemic tendency for \tilde{N}_e to be imprecise for the LD procedure when there is either insufficient sampling of individuals, loci, or both. Owing to stochastic effects in genetic drift and sampling error, mean values of the moment-based index approach theoretical expectations for large values of n_g and \mathcal{K} , where \mathcal{K} is the number of pairwise comparisons among \mathcal{K} independent alleles. Statistical precision for the goliath grouper estimate was evaluated by examining the coefficient of variation, CV, on \hat{N}_e as follows:

$$CV_{\hat{N}_e} = \sqrt{2/\mathcal{K}} \left[1 + \frac{3N_e}{n_g} \right]. \quad (6)$$

Because N_e in the numerator of the above expression denotes the true value, I conservatively used the upper confidence interval (CI) of the \hat{N}_e estimate in its place. The harmonic mean value of n_g was also used for the calculation, and \mathcal{K} was adjusted for missing data.

2.5. Life Table Synthesis

Data used to develop $s_{x,y}$ were extracted from the SEDAR 47 Final Stock Assessment Report [18]. The maximum age modeled here was $x_\omega = 37$ years. Male and female Von Bertalanffy growth function parameters were $L_\infty = 2221$ mm total length, $K = 0.0937$ year⁻¹, and $x_0 = -0.6842$ year. Natural mortality rates, M_x , were estimated using the Hoenig_{nlis} method [50], as described in the SEDAR 47 report, and $s_x = e^{-(M_x)}$. Whereas Bullock and Smith [23] estimated batch fecundity for two goliath grouper females to be $38,922,168 \pm 1,518,283$ and $56,599,306 \pm 1,866,130$ oocytes, robust age-specific estimates are unavailable. Thus, for fecundity estimation, the gonad weight-at-total-length relation-

ship was established as $GW_L = a + bL$, where $a = -36132.7$ and $b = 24.5$ [18]. Relative fecundity, b_{rel} , which is the mean number of eggs per gram of fish weight, was taken as 21,312 eggs/g [18]. Females were assumed to reach maturity at age 6, and female fecundity-at-age, $b_{x,f}$, was estimated to be $b_{x,f} = \rho_x(a + bL)b_{rel}$, where $\rho_{x,f}$ = proportion mature at age $x/100$. Owing to the absence of data for male fecundity, female values were adopted for males aged ≥ 6 years. For males aged 4 and 5 years, the approximation $b_{x,m} \approx \rho_{x,m}$ was used.

The quantity $b_{x,y}$ was scaled to constant N_{A+J} (for which $\bar{k}^* = 2$) using cumulative survival, $l_{x,y}$, through age x and sex y , where $l_1 = 1$ and $l_{x,y} = l_{x-1,y}s_{x-1,y}$ for $x > 1$ [25], with the scaled quantity denoted as $\dot{b}_{x,y}$. Finally, $B_{x,y}$, which is the estimated mean number of newborn births produced by all breeders of age x and sex y , was calculated as $B_{x,y} = \dot{b}_{x,y}N_{x,y}$. The effects of sex change were modeled in two ways. First, a fixed female-to-male ratio, $\overleftrightarrow{SR}_x$, of 1:1 was adopted for ages one to four and a simple linear function for female-to-male sex reversal was applied to the remaining age classes, such that $SR_{x,f} = 0.0061x + 0.5242$ for $x \geq 5$ years. Alternatively, a logistic function $SR_{x,f} = 0.754 + ((0.503 - 0.754) / (1 + (x/8.840)^{4.734}))$ for $x \geq 5$ years was surveyed to generate female age-specific sex ratios. The s-shape of the logistic function mimics the case where younger adult males transition at a greater rate than older males. For both functions, $SR_{x,m} = 1 - SR_{x,f}$.

For goliath grouper, empirical age-composition data were not sufficiently developed for a direct estimate of T [18], but the generation length has been previously reported to be $T \approx x_\alpha + ((x_\omega - x_\alpha)/2) \approx 21.5$ years, where $x_\alpha \approx 6$ years and $x_\omega \approx 37$ years. Here, I used a sex-specific measure of T that better accommodates the dynamic factors modeled, reflecting the average age of the parents of all newborn individuals in the modeled population. Estimates of T_y were computed during the course of hFHM runs via the life table equation:

$$T_y = \sum_{x_\alpha y}^{x_\omega y} [xB_{x,y}/N_1] \quad (7)$$

2.6. scFHM Runs

For base-model calibration (predictive scaling), exploratory values of $\check{N}_A = \{10,000, 35,000\}$ were combined with model-dependent input values of \check{s}_x , $\check{x}_{\alpha,y}$, and $\check{x}_{\omega,y}$ to determine \vec{N}_1 . The above \check{N}_A values were spatially explicit, intended to encompass adult goliath grouper residents of Florida Atlantic coastal waters. The calibration set used for predicting the Poisson scaling factor was $\check{\phi} = \{1, 25, 50, 150, 300, 750, 1500, 3000, 7500, 11,500, 15,000, 30,000, 75,000\}$. Predictions of $\vec{\phi}$ were performed using point estimates and upper and lower CIs of \check{N}_e .

In total, three biologically varying model constructions comprising six scFHM runs (78 hFHM runs) were implemented for the predictive phase (Table 2). For the base model, a gonochoristic reproductive strategy and a 1:1 sex ratio was assumed (M1). This model was then modified to accommodate the first diandric protogynous scenario (M2), incorporating the linear pattern of $SR_{x,y}$. Finally, the base model was modified to accommodate the second diandric protogynous scenario (M3), incorporating the logistic pattern of $SR_{x,y}$. Following the prediction of $\vec{\phi}$, 18 scFHM runs were implemented to establish levels of ψ , ψ^* , and related parameters for the population. Each of these runs were scaled with the predicted values of $\vec{\phi}$ for point estimates and upper and lower CIs of \check{N}_e .

Table 2. Model construction.

Model	Reproduction	Sex Ratio	N_A	N_1
M1A	gonochoristic	1:1	10,000 (fixed)	81,575 (tallied)
M1B	gonochoristic	1:1	35,000 (fixed)	285,526 (tallied)
M2A	diandric	linear increase in $SR_{x,m}$ with age	35,000 (fixed)	284,300 (tallied)
M3A	diandric	logistic increase in $SR_{x,m}$ with age	35,000 (fixed)	281,930 (tallied)
M2B	diandric	linear increase in $SR_{x,m}$ with age	35,150 (resultant)	285,526 (fixed)
M3B	diandric	logistic increase in $SR_{x,m}$ with age	35,446 (resultant)	285,526 (fixed)

3. Results

The total number of genotypes resolved for this Florida Atlantic study population was $n_g = 300$. Standard measures of genetic diversity are reported in Supplementary File S2. In total, $n_D = 45,451$ pairwise relationships were classified (including two intentionally replicated genotypes), a value that also represents the total probability mass of the empirical sampling probability distribution for r . The optimized $\mathbb{I}_{\mathcal{R}}$ was {IDP, 3.00; POP, 2.66; FSP, 33.68; HSP⁺, 88.39; FCP, 25.56; HFCP, 27.16; SCP, 46.84; HSCP, 373.44; URP, 44,850.27}, which represents the expected number of each categorical relationship pair given the data. Among those classified, 68 pairs of interest satisfied MAP_{50} assignment criteria (3 IDPs, 3 POPs, 35 FSPs, and 27 HSP⁺s). A parent–offspring triad consisting of two full siblings and a parent was inferred. Eight multiple-sibling families and an additional POP were inferred. The largest multiple-sibling pedigree consisted of six individuals that formed three FSP and six HSP⁺ relationships. Another 28 single-sibling families were credibly inferred, consisting of 15 FSPs and 13 HSP⁺s. Posterior probabilities of several additional pairs fell short of the MAP_{50} criterion, but their relationships were indicated by other robust familial assignments.

Fin-ray-based ages were assigned for 264 of the 302 specimens. The age compositions of all sampled specimens and members of classified close-kin pairs are depicted in Figure 4A. Most specimens, including those inferred to have paired familial relationships, were between the presumptive ages of 8 and 11 years at the time of their sampling. The minimum observed age was 4 years and the maximum observed age was 19 years. Age differentials between close-kin pairs appear in Figure 4B. FSPs differed in age by as much as 5 years, with the highest percentage (10 of 26) differing by only 1 year. HSP⁺s differed by as much as 11 years, with most differing by 2 years.

3.1. Effective Population Size Estimate

One genotype from each classified IDP was culled from the dataset prior to the estimation of N_e , yielding $n_g = 299$ for this analysis; the harmonic mean sample size was $n_g = 289.1$. Discounting monomorphic loci, there were 222 single-locus genotypes with missing data out of the (299×33) 9867 scored, yielding an overall genotyping efficiency of 98%. Accounting for missing data, the number of possible pairwise comparisons between k independent alleles was $\mathcal{K} = 43,456$. At $P_{crit} = 0.01$, a raw estimate of $\tilde{N}_e = 402.5$ was observed, with $CI = 359.3$ to 455.2. Upon bias adjustment for mixed-age sampling and physical linkage, $\hat{N}_e = 658.8$ ($CI = 588.1$ to 745.0). The estimated $CV_{\hat{N}_e}$ was 0.059, which was very low primarily owing to the large \mathcal{K} .

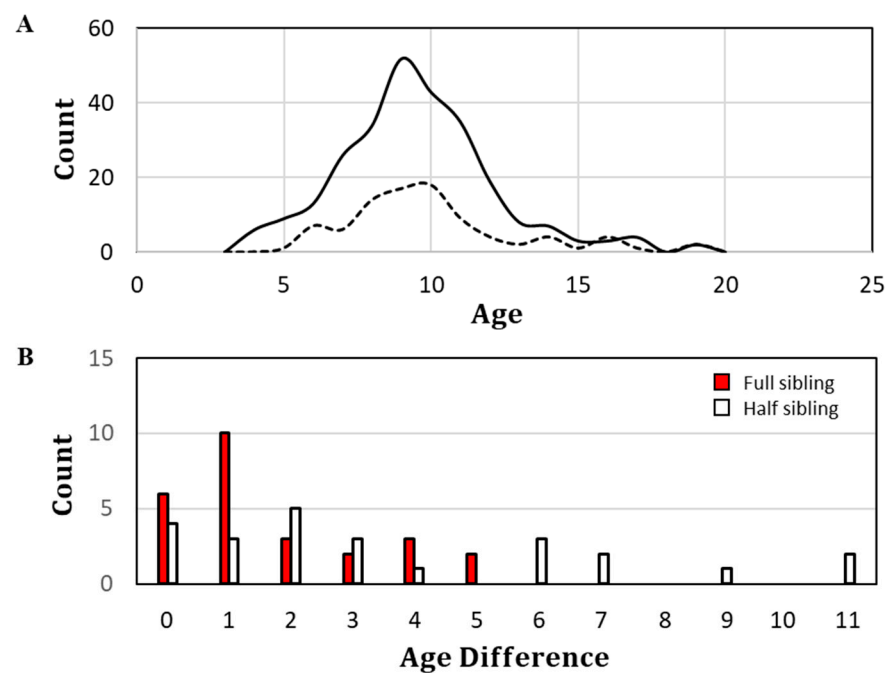


Figure 4. Age plots for the studied specimens of *Epinephelus itejara*. (A) Age composition. Solid line, all specimens; dashed line, specimens comprising close-kin pairs. (B) Histogram of absolute age differences among full- and half-sibling pairs.

3.2. Demographic Results

Life tables for all calibration models are provided in Supplementary File S3. Base model tallied values of \vec{N}_1 were 81,575 and 285,526 for \check{N}_A values of 10,000 and 35,000, respectively. However, when \check{N}_A was fixed at 35,000 during sex-reversal modeling, tallied values of \vec{N}_1 were 284,300 and 281,930 for M2A and M3A, respectively. Sex-specific population abundances for N_{A+J} and N_A are reported in Table 3. Estimates of \hat{T} are independent of modeled values of \vec{N}_1 . For the base model (M1), \hat{T} was estimated to be 20.99 years (Table 3). Whereas this model estimator was based on both fecundity and mortality, the result was comparable to the coarsely approximated value of 21.5 years based solely on x_ω and x_α . When M2 and M3 sex-reversal dynamics were incorporated, overall estimates of generation length decreased very slightly compared with those of M1. Expectedly, male T values were slightly higher than those of females (Table 3).

Table 3. Sex-specific and overall generation lengths and population abundances. Bold type denotes model input. Shaded area highlights differences between male and female abundances.

Model	M1A	M1B	M2A	M2B	M3A	M3B
\check{N}_A	10,000	35,000	35,150	35,000	35,446	35,000
\vec{N}_1	81,575	285,526	285,526	284,300	285,526	281,930
\hat{T}	20.99	20.99	20.90	20.90	20.92	20.92
\hat{T}_f	21.10	21.10	20.49	20.49	20.79	20.79
\hat{T}_m	20.89	20.89	21.31	21.31	21.05	21.05
$N_{A+J,m}$	60,737	212,591	214,147	212,928	218,335	215,585
$N_{A+J,f}$	60,737	212,591	211,033	210,429	206,845	204,242
N_{A+J}	121,475	425,182	425,182	423,357	425,180	419,827
$N_{A,m}$	6220	21,771	23,175	23,078	26,412	26,079
$N_{A,f}$	3780	13,229	11,975	11,922	9003	8921

The linear transition formula in M2 (Figure 5A) led to a relatively modest shift from the initial female-to-male $\overleftrightarrow{SR}_{x=1}$ to α of $\approx 1:1$ to that of $\overleftrightarrow{SR}_{x=38} \approx 1:2.25$. With a fixed value of \overrightarrow{N}_1 , this formula resulted in slightly more male breeders in the population and an overall adult female-to-male ratio of $\overleftrightarrow{SR}_{x=\alpha}$ to $\omega \approx 1:1.94$. Likewise, minimal change was observed when the value of \check{N}_A was fixed; $\overleftrightarrow{SR}_{x=\alpha}$ to $\omega \approx 1:1.94$. The logistic transition formula in M3 (Figure 5B) led to a somewhat higher shift; $\overleftrightarrow{SR}_{x=38} \approx 1:3.16$. Overall adult ratios for M3 were $\overleftrightarrow{SR}_{x=\alpha}$ to $\omega \approx 1:2.93$, respectively, whether \overrightarrow{N}_1 or \check{N}_A were fixed.

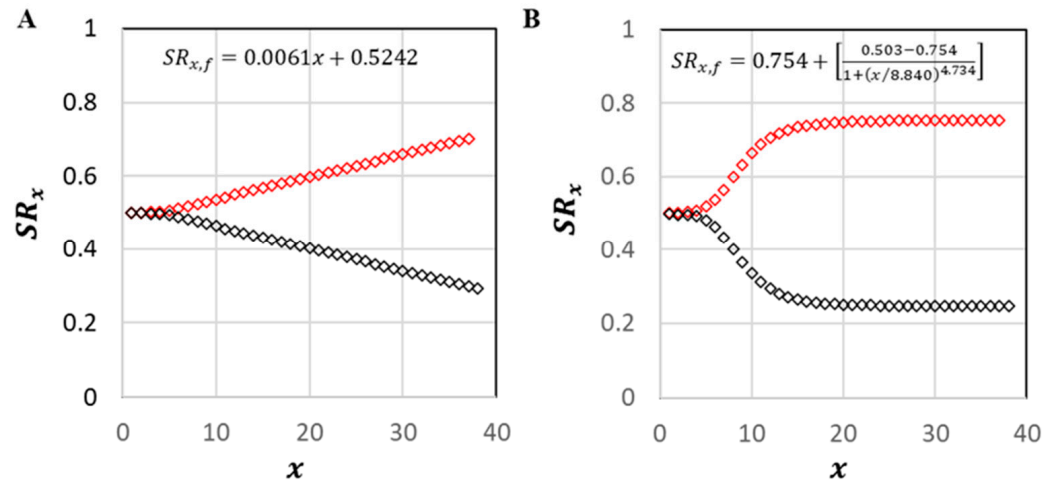


Figure 5. Modeled age-specific sex-reversal transitions for *Epinephelus itejara*. Red markers, male sex ratios; black markers, female. (A) Linear M2A/B dynamics. (B) Logistic M3A/B dynamics.

3.3. Reproductive Success Metrics

All best-fit predictive curves from the logistic regression were recovered with high precision ($R^2 > 0.999999999999$). Robust predictive behavior was not unexpected given the underlying deterministic process model. Thus, $\overrightarrow{\phi}$ can be extrapolated in predictive plots with sufficient accuracy (Figure 6) during workflow step 3.2 (Figure 2).

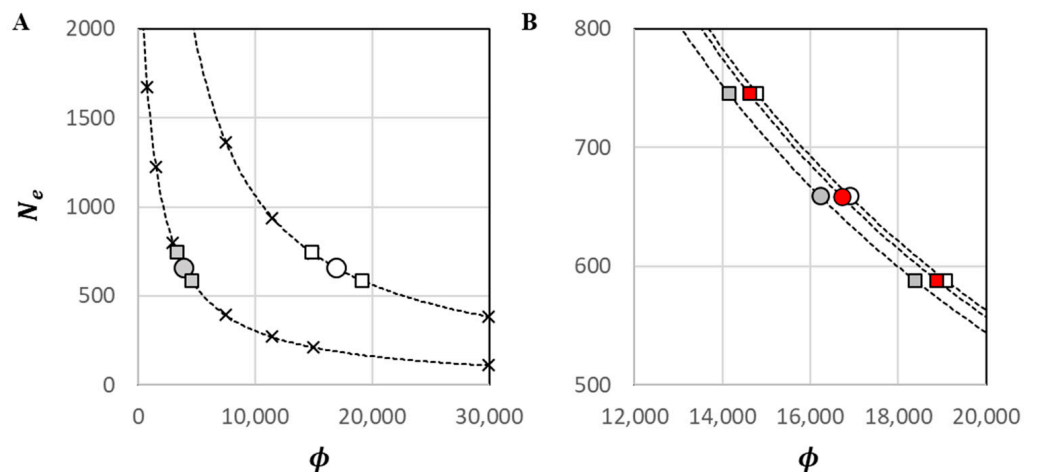


Figure 6. Predictive plots for inferred values of $\overrightarrow{\phi}$. Dashed lines depict predictive functions for \check{N}_e at $\overrightarrow{\phi}$; circles depict $\overrightarrow{\phi}$ based on the \check{N}_e point estimate; squares depict $\overrightarrow{\phi}$ based on upper and low CIs of \check{N}_e . (A) 'x' = calibration points from the set $\{\check{N}_e$ at $\overrightarrow{\phi}\}$; grey symbols = M1A; white = M1B. (B) White symbols = M1B; red = M2B; grey = M3B.

In scaled-model runs (step 4.1 of the scFHM workflow; Figure 2), all three model constructions were first evaluated with common values of $\vec{N}_1 = \{81,575; 285,526\}$ and model-specific $\vec{\phi}$ values. They were then evaluated with common values of $\hat{N}_A = \{35,000\}$ and model-specific $\vec{\phi}$ values (see Table 2). Overall, levels of ψ and ψ^* were very high and positively related to modeled values of \vec{N}_1 (Table 4). Based on the point estimate for \hat{N}_e , inferred values of \hat{V}_k and \hat{V}_k^* for goliath grouper were extremely high, ranging from 5354 to 22,811 for \hat{V}_k and from 10,395 to 36,390 for \hat{V}_k^* . Values of \hat{N}_b were very low, ranging from 17.2 to 40.9. The incorporation of sex reversal had a minimal reductive effect on those variance estimates, by way of a reductive effect on ϕ , and a minimal but enlarging effect on the effective number of breeders. The effects were greater in M3 than in M2 and greatest in M3B. Calibration data for $\hat{\phi}$ predictions; parameter values for logistic equations; and final scFHM estimates of \hat{k}^* , \hat{V}_k^* , \hat{N}_b , \hat{k} , and \hat{V}_k based on upper and lower CI values of \hat{N}_e are provided in Supplementary File S3.

Table 4. scFHM results for each model construction.

	Model	M1A	M1B	M2A	M2B	M3A	M3B
Input	\hat{N}_A	10,000	35,000	35,151	35,000	35,446	35,000
	\vec{N}_1	81,575	285,526	285,526	284,300	285,526	281,930
	\hat{N}_e	658.77	658.77	658.77	658.77	658.77	658.77
	$\vec{\phi}$	3898.64	16,896.17	16,781.89	16,703.58	16,454.12	16,226.14
ARS	\hat{V}_k	5354	22,811	22,661	22,556	22,252	21,946
	$\hat{V}_{k,f}$	5356	22,812	22,852	22,746	22,947	22,632
	$\hat{V}_{k,m}$	5352	22,809	22,473	22,369	21,595	21,297
	\hat{k}	1.34	1.34	1.34	1.34	1.34	1.34
	\hat{k}_f	1.34	1.34	1.35	1.35	1.38	1.38
	\hat{k}_m	1.34	1.34	1.33	1.33	1.31	1.31
	\hat{N}_B	40.9	33.6	33.8	33.9	34.5	34.5
	$\hat{N}_{B,f}$	20.5	16.8	16.9	16.9	17.2	17.2
	$\hat{N}_{B,m}$	20.5	16.8	16.9	16.9	17.3	17.3
	ψ	2677	16,985	16,874	16,795	16,569	16,341
	ψ_f	2678	16,986	16,890	16,811	16,628	16,400
ψ_m	2676	16,984	16,859	16,781	16,510	16,282	
LRS	V_k^*	10,395	36,390	36,233	36,077	36,267	35,811
	ψ^*	5198	18,195	18,117	18,038	18,134	17,906

4. Discussion

Here, a scaled version of Waples et al.’s [25] hybrid Felsenstein–Hill model was used to infer sex-specific estimates of reproductive success metrics that, within the context of relevant demographic rates and measures, were consistent with an independent estimate of N_e . To the best of my knowledge, the empirical N_e estimate for this Florida Atlantic population represents a first documentation of effective population size for goliath grouper. The very low observed value of N_e was associated with highly overdispersed variance in lifetime and annual reproductive success. Indeed, the modeled level of ψ^* exceeded by two orders of magnitude those inferred for red drum and southern bluefin tuna. The model results were only minorly impacted at both annual and lifetime scales by the inclusion of sex reversal dynamics, as will be reviewed in the following section.

The interpretation of results for this particular application of the hFHM relies on a host of factors, but a major limiting factor appears to be the rigorous individual and allelic sampling requirements for empirical N_e estimates, which have rarely been met in past studies of large marine populations (see also [49]). For goliath grouper, a large number

of moderately polymorphic loci were genotyped, permitting more than 43,000 paired comparisons of \approx independent alleles. The number of the individuals surveyed was of the same magnitude as the N_e estimate itself, which satisfied a general guideline from Waples [49]. As a result, the coefficient of variation for the N_e estimate was very low, suggestive of good precision. Empirical precision was also reflected in the upper and lower CIs, which were close in value to the point estimate. Thus, it appears the estimate for the time period to which it applies was sufficiently precise so as to robustly support the study findings and conclusions. Other empirical approaches exist for estimating N_e (reviewed in [51]) that carry conditions and assumptions that require careful consideration. It should be noted that empirical estimates of N_B , when available, can also be used to predict ϕ .

The choices of N_A explored in the model may seem low at a glance, but for two aspects. First, the empirical estimate of N_e used to scale the model is a generational estimate that applies to the reproductive successes of the parents of study specimens, which were alive and breeding back when adult abundances in the Florida Atlantic region were considerably lower. This aspect will be discussed further in Section 4.2 in regard to kinship structure. Second, when N_e is treated as a known value in the scFHM workflow, the magnitudes of ϕ and V_k scale with the tallied value of N_{η} , which increases when larger values of N_A are modeled. If the exploratory values of N_A were indeed too small, it would only serve to heighten ramifications for CKMR associated with the very high levels of overdispersion.

A new genetic survey by FWC scientists of sampled-and-released adult and juvenile goliath grouper is currently underway in both the Florida Atlantic and Florida Gulf of Mexico, starting in 2019. Those data, when they become available for analysis, will provide an opportunity to determine whether reproductive success dynamics have improved over the interval period.

4.1. Influences of Fishing Pressure and Sex Reversal

The absence of information on possible compensatory or depensatory responses precluded a direct examination of fishing pressure effects, alone and in conjunction with sex reversal. Nonetheless, general impacts of harvest on reproductive success dynamics are predictable. Even when compensatory responses maintain N_{η} , harvest can lead to decreased generation lengths through the loss of older individuals [52,53] and perhaps earlier maturation [54]. N_e would be expected to decrease with reductions in T caused by age truncation and be exacerbated further by earlier maturation [38,55]. In populations lacking a compensatory reserve [56] and/or subject to depensatory responses, fishing mortality could simultaneously reduce V_k^* , which could offset changes to N_e caused by reductions in T , so the effects must be modeled jointly.

In diandric protogynous populations, some members are born as primary males while others transition from females to secondary males during adulthood, presumably in response to social, behavioral, or environmental cues [57]. Under intense fishing pressure, sex reversal rates can also be a product of compensatory density dependence. Given these circumstances, male abundance, fertilization success, and stock productivity can all be affected by the spatio-temporal dynamics of asynchronous transitioning. Certain forms of selective harvest can skew population sex ratios in a manner that reduces reproductive potential [58–60]. For example, in gag (*Mycteroperca microlepis*), sex change is believed to occur mostly (but not entirely) within the pre-spawning habitat. This habitat seems to represent a critical source of male recruitment to the spawning grounds, where many males are believed to become year-round residents. High fishing pressure in pre-spawning habitat areas, while at the same time also causing age truncation, appears to have played a role in the current female-to-male $\overset{\leftrightarrow}{SR}$ in the eastern Gulf of Mexico, which has been estimated to be $\sim 49:1$ [61]. Gag likely represents a somewhat worst-case circumstance within the grouper–snapper complex of Serranid fishes [12].

Neither Bullock et al. [10] nor Koenig and Coleman [11] found evidence that the adult $\overset{\leftrightarrow}{SR}$ of goliath grouper differs significantly from 1:1. The resultant sex ratios from M2A/B and M3A/B were thus not consistent with the above field observations, as they resulted

in ~1:2 and ~1:3 adult female-to-male ratios, respectively. More research data on the true sex reversal dynamics of goliath grouper are needed for a species-specific assessment. In both models of sex reversal investigated here, increases in T for males were offset by decreases for females such that the overall estimated generation lengths did not differ meaningfully from that of the base model (Table 3). M2 and M3 sex reversal dynamics resulted in only very small decreases in V_k in comparison with M1B, with the more extreme (logistic) transition pattern (M3) showing the greatest reduction. These decreases were associated with reduced values of \vec{N}_1 (Table 4). Consistent with the variance decreases, values of N_B showed corresponding but slight increases in M2 and M3.

Under fully identical male and female demographic rates and conditions ($s_{x,m} = s_{x,f}$, $b_{x,m} = b_{x,f}$, $x_{\alpha_m} = x_{\alpha_f}$, and $x_{\omega_m} = x_{\omega_f}$), it would be expected that sex reversal would have minimal, if any, enlarging effects on V_k and V_k^* , and thus very slight reductive effects on N_B and N_e . However, modeled maturity schedules and age-specific fecundities were not the same for goliath grouper males and females. Because $s_{x,m} = s_{x,f}$ and $x_{\omega_m} = x_{\omega_f}$ in all goliath grouper models, the minor differences observed between M1B and M2/3 and their directional effects must have been associated with earlier maturation in males. For the most part, sex-specific changes in reproductive success metrics of goliath grouper caused by sex reversal were offsetting, such that overall values (male + female) of ψ were not greatly affected. These results suggested that sex reversal itself will not have a significant impact on V_k , V_k^* , N_B , or N_e for goliath grouper unless it is accompanied by aggravating factors that significantly and disproportionately alter fecundity and/or mortality in a sex-specific manner, such as the size-selective fishing previously discussed for gag. The offsetting tendencies and sensitivities to aggravating factors are expected to be similar for protandrous hermaphroditic fishes (e.g., common snook, *Centropomus undecimalis* [62]).

4.2. Kinship Distribution and Spatial Dynamics of Close Kin

It would be a reasonable a priori expectation that the prevalence of full siblings (and other 'full' relations) would be quite low in natural populations of iteroparous species with indeterminate fecundity, especially broadcast-spawning species whose members aggregate over protracted spawning seasons and repeat this over decadal time scales. Therefore, some may find it surprising that so much of the optimized sampling probability mass was assigned to full-sibling relationships (nearly one-third of that assigned to presumptive half-siblings). Whereas other grouper species (e.g., gag and red grouper, *Epinephelus morio*) are known to spawn in pairs, it has been posited based on male gonad size and sperm quantity that goliath grouper spawn in multi-male groups [22]. That may indeed be the evolved strategy, applicable when the temporospatial availability of breeders permits it. However, the only documented direct observation of goliath grouper spawning involved one female and only two males [22]. If it was true that females were accompanied more frequently than presumed by only a few males during their "spawning rushes" to the surface, it would not be unusual to have encountered littermates among offspring within year classes. Still, given the lengthy reproductive lifespan of adults, a somewhat high prevalence of cross-year-class FSPs is harder to reconcile biologically without evoking circumstances of frequent paired mating, very high spawning site fidelity, or other special circumstances.

At the times and places that sampling occurred for this study (Figure 3), spawning aggregations often consisted of ~15–20 individuals, although the mean value was likely negatively biased owing to inclusion of non-spawning sites in the survey design [22]. Specimens were collected from ongoing reproductive studies and were not products of a random sampling design. Nonetheless, supposition by SEDAR 47 panel members that goliath grouper populations were age-truncated [18] was generally supported by the age composition of sampled specimens, whose maximum observed age among the 264 aged fish was $x = 19$ (Figure 4A). Procedures for fin-ray ageing for goliath grouper were established in Murie et al. [41]. In that study, there was only 67% overall agreement between two independent readers. Agreement improved to 89% for independent readings within ± 1 year and to 100% within ± 2 years. The close-kin findings in the present study were

suggestive of ± 1 ageing error, albeit to an unknown degree (Figure 4B). However, even if it were assumed that all inferred FSPs with ≤ 1 year age differentials are littermates, nearly 40% of the full siblings still had age differentials ≥ 2 years and likely belonged to different cohorts, as did the majority of presumptive half siblings.

In terms of relationship classification error, analytical false rejections and detections were possible, as well as non-analytical false rejections. Without formulaic error tolerance, IDP and POP relationships are subject to de facto exclusion (i.e., non-analytical false rejection) when at least one member of the pair is mistyped. Conversely, mistypings do not result in de facto exclusions for FSPs or HSP⁺s, they only reduce posterior probabilities, and to a small degree when m is large. Thus, even when reductions in $P(\mathcal{R}_i | \mathbb{E}, \mathbb{I})$ occur, the evaluation could still result in an accurate MAP classification, depending on the decision rule. When genotyping error is low, the majority of occurrences in multiple-comparison applications are ‘silent’—i.e., they do not involve members of close-kin pairs. Mutations represent another source of type II error for POPs, FSPs, and HSP⁺s but, again, without de facto exclusion and with the majority of occurrences being silent. Lab error and mutation were not expected to result in a significant number of misclassifications in this study. Analytically, given the very high burden on \mathbb{E} for overcoming \mathcal{R}_{UR} in $\mathbb{I}_{\mathcal{R}}$, it was more likely that a portion of true close-kin pairs (predominantly HSP⁺s) were falsely rejected than falsely detected, and to the extent that false rejections occurred, the conclusions of the present study would be strengthened.

So, how can these kinship dynamics be explained? First, focus must be shifted to the adult abundance at the time that parents of the classified sibling pairs were breeding. The age composition of sampled specimens was dominated by age classes 8 to 11 and the ages of the members of sibling pairs were generally similar (Figure 4A). Accordingly, many of the full-sibling-pair members would have had birth dates during the late 1990s or very early 2000s—i.e., during a period when Florida Atlantic spawning aggregations still comprised only a few individuals and their spatial distributions were sparse (see Figure 2 of [22]). The above demographic circumstances are consistent with scFHM estimates of \hat{N}_B , which suggested, population-wide, that reproductive contributions to annual cohorts during that period were dominated by only ~17 to 20 adult males and females, respectively (Table 4), and that zero-inflation was potentially a factor in the scale of overdispersion [63].

Second, spawning-site fidelity in adult goliath grouper appears to be very high (>75–80%), at least over a period of a few consecutive years [19]. So, during that period, it is not unlikely that dominant breeders returned to the same few spawning sites and the same small spawning groups over a period of years. Regarding zero-inflation, there is also the possibility that some spawning sites in the region are not suited to larval retention if, for example, those spawned at certain deep-water offshore sites became entrained in the powerful northward surface flow of the Florida Current [64] and settle in the South Atlantic Bight [65] or elsewhere. Two POPs were identified in this relatively small population genetic dataset, indicating that recruitment can be localized to a degree. However, if a component of the Florida Atlantic larval supply is subject to unidirectional exportation, then entire annual and perhaps lifetime reproductive contributions of certain site-faithful breeders could be ‘lost’ to the Florida Atlantic population, with the resulting zero-inflation contributing to both ψ and ψ^* .

It is not unexpected that half siblings would be observed over a broader range of age differentials than full siblings (Figure 4B). If either parent suffers mortality, no additional full siblings can be produced, but half-sibling production remains possible through the surviving parent. Likewise, if successful female breeders transition to male breeders, they can no longer produce full siblings to any offspring produced prior to sex reversal, while half siblings remain possible. Under all or most of the above conditions and circumstances, the kinship distribution observed for this particular sample becomes plausible, especially when coupled with the potential for intrinsic forms of persistent individual differences in LRS [66].

Given that the observed kinship distribution is plausible, a new hypothesis—i.e., that kinship dynamics have responded to continued population expansion—becomes testable through investigation of the younger year classes now being surveyed by FWC. The alternate hypothesis in this case would reflect a return toward expected dynamics—i.e., fewer FSPs relative to HSP⁺s in the distribution, as well as FSP plus HSP⁺s jointly comprising a significantly smaller proportion of the total sampling probability mass. However, if the dynamics have not changed, it could suggest that the Florida Atlantic population is indeed a net exporter of its reproductive potential and is largely sustained by the local contributions of comparatively few adults, perhaps with occasional immigration and/or larval import from the Florida Gulf.

4.3. Implications of Spatial Structure for CKMR

Preliminary plans for goliath grouper CKMR call for a POP-proxy-based design, with sampling currently focused on both adult and juvenile populations. Estimation could be extended to HSP⁺s if a DNA-based method of ageing is developed [67] and if other technical/analytical hurdles can be overcome. Spatial structure, where reproduction is concentrated in certain geographic locations, will not create bias in CKMR estimates either when dispersal is population-wide (complete mixing exists) or when adult sampling is not spatially biased. Under a hypothesis of “complete mixing”, fish are considered sufficiently dispersed when the expected distance between closely related individuals is approximately equal to that of randomly chosen unrelated individuals. In that case, it would not matter if sampling were spatially non-random and opportunistic sampling can provide unbiased estimates. However, when dispersal distances are limited, abundance estimates are expected to be negatively biased when adult sampling is non-random [3,5]. Negative bias can also occur when dispersal is unidirectional.

Both home-site and spawning-site fidelity in adult goliath grouper appear to be very high, although the distances between home sites and spawning sites, owing to a spatial concentration of the latter, can be large [19]. Larval dispersal is expected to be complex and potentially broad, given the lengthy pelagic larval duration (Table 1). Kinship spatial structure and geographic linkage between spawning and recruitment will be better understood when enough POPs are mapped in relation to randomly selected unrelated pairs. Given POP-based proxies, the a priori sampling design for goliath grouper adults should seek to be spatially representative to the extent possible and include both home sites and spawning sites. POP linkages with Florida Gulf specimens have not yet been observed, although two second-degree relationship pairs have been (M.D. Tringali, unpublished data). Because of limited demographic connectivity of goliath grouper between the Florida Atlantic and Gulf coasts [19], spatially explicit estimates may be required. Larval exportation out of the Florida Atlantic population into unsampled areas must also be considered. Sampling of juveniles, apart from having broad and bi-coastal representation, need not to be fully random and should be focused on sample size sufficiency while avoiding conditions and tactics that would favor sampling of littermates.

4.4. Ramifications of Family-Size Variance for CKMR

As expected, levels of ψ and ψ^* were sensitive and positively related to modeled values of \vec{N}_1 at the given value of \hat{N}_e . Nonetheless, even at the lowest modeled newborn abundance values, variances in ARS and LRS were extremely high. Moreover, estimated values of $\hat{N}_B \approx 30$ to 40 were extremely low in comparison with those for southern bluefin tuna ($\hat{N}_B \approx 79,000$ to 120,000 [68]), which has become the exemplar marine fish species for CKMR. As noted, inferences of numerous multi-sibling families among ~120 close-kin classifications were consistent with the extremely high family-size variance elicited from scFHM results, and both represent a ‘red flag’ for CKMR application. Should relatively few goliath grouper parents continue to dominate reproduction, the observed numbers of parent–offspring matches in a CKMR analysis would vary widely depending on whether the prolific parents are sampled, thus the assumption of juvenile independence would be

violated [3]. Quantifying the impact on precision would likely require individual-based modeling. Unfortunately, the only remedy for this loss of precision would be an increased investment in sampling, both in annual specimen numbers and collection years, which may not be practical in an unharvested or minimally harvested population.

It should be noted that values of V_k and \hat{V}_k^* will differ when estimated using the abundances of different pre-reproductive age-classes, so the ages at which offspring in POPs are collected must be considered. For \hat{V}_k^* , because \hat{N}_e and \hat{T} are static in this model workflow, differences in \hat{N}_η must be offset by nearly proportional changes in variance. Generation length is not a factor in annual variances. However, given the linkage of \hat{N}_B to \hat{N}_e in the deterministic model, proportionality between \hat{N}_η and $\hat{\psi}_\eta$ is also expected.

For multi-year studies, parental mortality must be taken into account. As mentioned, if analyses were to be extended to cross-year half-sibling matches as proxy recaptures, there are additional complexities. When half-sibling pairs from different year classes serve as CKMR proxies, age-specific mortality must also be accounted for and thus some method of non-lethal ageing is required. Other factors, such as changes in fecundity with age and other 'BOFFFF' effects [69,70], skipped spawning, and persistent individual differences in reproductive success [66,71,72], can also affect estimation [5] if not evaluated (or modeled) quantitatively and corrected in silico.

As a result of the study findings presented here, potential impacts from ψ on the precision in CKMR-based abundance estimates cannot be neglected. The ongoing genetic surveys in the Florida Atlantic and Gulf coastal populations will permit a more thorough and timely view. If the unfavorable biological conditions indicated in the present data have not significantly improved, alternatives to CKMR must be considered. For example, proxy-associated problems could be circumvented altogether by instead searching the genetic data instead for IDPs and adopting an individual-based method of GCMR, with multi-year open-population extension, such as multi-state super-population modeling [73] or multi-state open robust design [74]. Multi-state capture–mark–recapture approaches are flexible in cases of transience or temporary emigration, and when individual heterogeneity in capture probability is expected. Precision of estimates, as with any individual-based mark–recapture approach, would be largely dependent on the robustness of sampling with respect to capture probabilities, with both multi-state GCMR approaches being somewhat forgiving to sampling designs and adaptable to ongoing sampling. In this application, however, in silico adjustment for handling mortality would also be required. Close-kin pairs identified within the same genetic database would remain useful to the extent that they contribute to the understanding of spatial patterns and dynamics in dispersal and recruitment, which remains a critical information need.

4.5. Conservation Genetic Implications

Natural selection and gene flow are directional evolutionary forces, often referred to as countervailing (or balancing) linear pressures. Genetic drift, on the other hand, is a directionally unpredictable force—one that counteracts and possibly disrupts the other two [75]. The intensity of drift is directly related to N_e , such that 'effective neutrality' of genetic variants can be assumed when selection coefficients are quantitatively less than $(1/(2N_e))$ [76]. As a result, when N_e is very small (i.e., <200–300), natural selection may fail to purify much of the newly arising (or imported) detrimental variation or to perpetuate beneficial mutations [77]. Over time, selective environments change and small effective population sizes can also impose limits on the rates of environmental change at which populations remain viable [78]. Drift is a threshold dynamic—i.e., N_e needs only to be 'large enough' for its influence to become de minimus. Beyond providing a temporal cushion, additional conservation genetic gains are not derived from N_e being a lot larger than large enough.

Using reproductive success metrics that should be familiar to the reader at this point, geneticists quantify 'opportunity for selection' as $I = V_k^* / (\bar{k}^*)^2$ [28,79–81]. Selective opportunities that arise from overdispersed family-size variance are important for repro-

ductive resilience and population persistence. However, although increased opportunities for selection imply a greater potential for evolutionary change, the index above, as pointed out by Waples and Reed [63], does not quantify selection itself. One of the things that matters is the degree to which the associated trait variance is driven by random effects. So, the question becomes, can reproductive strategies be adaptive [82] even when reproductive success is very strongly skewed toward a relatively small fraction of potential breeders and variance in that success is extremely high?

As it turns out, adaptation may indeed be possible under those circumstances (in theory, at least) through a mechanism involving recurrent and pervasive selective sweeps of beneficial mutations that arise as a consequence of enormous life-long fecundities [83]—another possible benefit of the “small-eggs” strategy [84]. Individuals carrying these mutations pass through numerous independently acting selective filters during their development toward reproductive maturity, with the cumulative result being highly variable and skewed offspring distributions and genetic constitutions of survivors that differ from those of non-survivors. Here, I refer to the ‘recurrent selective sweepstakes’ hypothesis as RSS to distinguish it from the ‘sweepstakes reproductive success’ hypothesis [85], commonly known as SRS—the two concepts are quite different. Despite what SRS might portend, lifetime reproductive success need not be a ‘jackpot’ system in which natural selection is a bystander while winners and losers are determined by random extrinsic forces. Instead, the reproductive resilience displayed by many marine populations and the diversification of their reproductive strategies indicate that they have adapted to persist over ecological and evolutionary timescales despite high-birthrate, high-early-mortality (type III) survivorship in challenging and patchy environmental conditions.

For the recurrent sweeps imagined by RSS to happen, positive selective forces must remain pervasive and strong. The N_e/N_A ratio, which is the sole qualifying metric for SRS [86], is not particularly meaningful with respect to the assessment of RSS, but associated variables are. That is, N_H , which is linked to reproductive potential [87], must remain consistently large enough to provide a steady supply of beneficial mutations. N_e must (only) remain consistently large enough so that selection is not derailed by the effects of drift. V_k^* must provide sufficient ‘opportunities for selection’ and, in some cases, it may also be beneficial when T is long enough to afford breeders that continue to survive under challenging environmental conditions additional reproductive opportunities to achieve LRS.

Recently, an RSS hypothesis based on the Durrett–Schweinsberg coalescent model was shown to provide the best explanation for observed site-frequency spectra patterns in whole-genome sequences of Atlantic cod, *Gadus morhua* [83], outperforming a ‘random sweepstakes’ (Xi-Beta coalescent) model that mimicked the SRS concept. Spectra patterns of differently sized fragments (25 kb, 100 kb, whole genome) and various functional classes (e.g., 4-fold degenerate sites, introns, exons, promoters, 3-UTRs, and 5-UTRs) all maintained best fit to expectations of the Durrett–Schweinsberg coalescent model. The RSS hypothesis will not apply universally to marine populations. However, unlike SRS, it is fully compatible with the broader ‘reproductive resilience paradigm’ of Barbieri et al. [82] and provides an intuitively sensible alternative to SRS for those populations that consistently operate under high levels of ψ^* .

The above considerations underscore the importance of monitoring fishery stocks for genetically secure effective population sizes. Technology and analytical insight [6,49] is allowing us to move beyond decades of underestimated N_e values, to the degree that effective population size will probably not be a forefront conservation concern for most large, natural (i.e., unstocked) populations of long-lived marine fishes. However, when it is a concern, it should not be neglected—or exacerbated. Following severe overfishing or other mass mortality events (e.g., red tides and cold kills), the best management approach for populations having non-secure effective sizes may be to manage the stressors where possible and patiently allow the fish to exercise their evolved reproductive resilience. Stock ‘restoration’ via captive propagation and release can have large and undesirable reductive

effects on N_e [88–91] and also replaces the critically important selective filters operating on early life stages with unnatural and counterproductive ones [92,93]. Stocking should be avoided in population-crash scenarios [94] unless circumstances become dire enough that short-term demographic risks outweigh forecasted intermediate- and long-term genetic impacts, or unless ‘genetic rescue’ from inbreeding depression becomes necessary [95].

5. Conclusions

In this study, I have shown that the highly overdispersed reproductive success dynamics modeled for this population and its atypical kinship distribution have important ramifications for planned close-kin mark–recapture analyses. Unless and until it can be demonstrated that the observed dynamics have improved, the use of CKMR is not recommended as a tool to estimate abundance for goliath grouper in Florida Atlantic waters. Fortunately, other genetic-based methods exist, and these should be considered. Furthermore, most conservation geneticists agree that $N_e \geq 500$ is required for long-term genetic security and population viability [78,96], especially for organisms such as marine fishes with very high reproductive rates [97]. It appears that, for goliath grouper in Florida Atlantic waters, the effective population size had reached a point in previous generations where it was at or just above that critical threshold. This condition warrants continued monitoring.

Supplementary Materials: The following supporting information can be downloaded at <https://www.mdpi.com/article/10.3390/fishes8050254/s1>. Supplementary File S1: Partial life tables to tally N_1 (MS Excel); Supplementary File S2: Molecular protocols and procedures (MS Word); Supplementary File S3: Final life tables and calibrations (MS Edge HTML). References [47,48,98–104] are cited in supplementary materials.

Funding: This research was funded by the State of Florida and the Department of the Interior, U.S. Fish and Wildlife Service, under the Federal Aid in Sport Fish Restoration Program, Grant F-69 to Michael Tringali, FL FWC. Tissue collections were funded by NOAA MARFIN grant NA10NMF430123 to Chris Koenig and Felicia Coleman, FSU.

Institutional Review Board Statement: Non-lethal tissue collections from live specimens were conducted by FSU colleagues in accordance with institutional and national guidelines concerning the use of animals in research, as approved by the Institutional Animal Care and Use Committee (IACUC) through FSU Protocol #1106.

Informed Consent Statement: Not Applicable.

Data Availability Statement: Data and information needed to evaluate the conclusions in the paper are present within the paper, cited literature, Supplementary Materials, and/or public repository. The genotype dataset used in this study for relationship inference and N_e estimation in goliath grouper, as well as posterior predictive distributions for all paired relationship inferences ($n_D = 45,451$), are available from the author upon reasonable request.

Acknowledgments: A special thank you to Felicia Coleman for organizing and guest editing this special issue on goliath grouper. Chris Koenig was a valuable source of information on goliath grouper reproductive biology. Cecilia Puchulutegui and Nathan Van Bibber genotyped all specimens. I thank Mike Norberg for cartography, Nancy Sheridan for helpful pre-submission comments, and photojournalist Walt Stearns; <https://sfups.org/photo-galleries/walt-stearns/> (accessed on 23 March 2023) for the photograph in Figure 1. Genetic samples from the majority of specimens were kindly provided by the FSU Coastal Marine Laboratory; appreciation is extended to Chris Malinowski, Angela Collins, and all who assisted in collections.

Conflicts of Interest: The author declares that he has no known competing financial interests or personal relationships that influenced or could have appeared to influence the work reported in this paper. All statements, findings, conclusions, and recommendations are those of the author and do not necessarily reflect the views or policies of the U.S. Department of Interior. Mention of trade names or commercial products does not constitute their endorsement by the author or the U.S. Government.

Appendix A. Statistical Framework for Close-Kin Classification

Nine possible categorical relationships, \mathcal{R} , were considered for the present analysis and specimen pairs were assigned probabilistically to these categories using a Bayesian genealogical approach. Because some specimens were released after capture, the ‘identity’ relationship, ID, was retained in the analysis to screen for cases of individual resampling. The eight remaining relationship categories considered were as follows: parent–offspring (PO), full sibling (FS), half sibling/avuncular/grand (HS⁺), first cousin (FC), half-first cousin (HFC), second cousin (SC), half-second cousin (HSC), and unrelated (UR). When discussing related pairs of individuals, the above designations are appended with ‘P’; e.g., HSP⁺.

The statistical framework for genealogical inference here builds on previously reported likelihood-based models (e.g., [105]) but, as will be shown, extends generality for the exploration of a multitude of empirical questions, including those involving complex circumstances. Bayesian approaches can be explicitly framed to address specific empirical questions by asking, what is the probability, P , that a research hypothesis, $H_{\mathcal{R}}$, is true, given the evidence, E , and conditioning information, I , relative to a null hypothesis, $\hat{H}_{\hat{\mathcal{R}}}$? The approach ultimately casts the categorical relationship ensemble as a mixture model and adopts a stochastically approximated process prior to multiple comparisons. The hypothesis-driven framework formulated here is general to all categorical forms of relationship inference for pairs. It involves the evaluation of the posterior probability $P(\mathcal{R}|E, I)$ that a hypothesized relationship \mathcal{R} is true for a pair, given the observed genetic evidence \mathbb{E} from some total compared number $\mathbb{G}_{X,Y}$ of genotyped pairs, such that $\mathbb{E} = \{E_n\}_1^{\mathbb{G}_{X,Y}}$, and a conditioning variable I , relative to a mutually exclusive ‘null’ hypothesis $\hat{\mathcal{R}}$. The null term $\hat{\mathcal{R}}$ implies ‘all else except \mathcal{R} ’, and thus necessitates a sufficient joint evaluation of plausible competing hypotheses. The consideration of all plausible probability space is curiously underappreciated in existing formulations and approaches. That is, for model specification, it must be assumed within the context of a categorical probability distribution that the interval of \mathcal{R}_i rival relationships for the set $\{\mathcal{R}_i\}_1^r$ is sufficiently representative [106] of the total probability space, such that $\sum_{i=1}^r [P(\mathcal{R}_i|E_n, I)] \cong 1$. As such, the framework described herein may be characterized as heuristic except for those applications involving strictly controlled mating designs, for which $\sum_{i=1}^r [P(\mathcal{R}_i|E_n, I)] = 1$.

The base likelihood function $P(E|\mathcal{R})$ is evaluated as described below (Appendix B) to obtain the conditional probability of obtaining y given the research hypothesis. The prior probability $P(\mathcal{R}|I)$ refers to the probability that the research hypothesis is true independent of the (new) genetic evidence. Within this framework, the set $\{P(\mathcal{R}|I)\}$ for a given evaluation may be analogous to the corresponding set of empirical sampling probabilities $\{\mathcal{F}_{\mathcal{R}}\}$ of the rival relationships with cardinality $|\mathcal{r}|$, which are taken to be constant over multiple comparisons. Accordingly, $\{P(\mathcal{R}|I)\}$ can be based on naïve or explicit prior information or optimized iteratively by empirical Bayes estimation during the course of an experiment or study (Appendix C). A Bayes classifier, informed by the maximum a posteriori probability (*map*) estimate [107], is available. That is, for each pair, one of the evaluated relationships will attain plurality with respect to the total probability mass as the posterior mode of the joint distribution of all plausible hypotheses (Appendix D). Using top-down filtering, the classifier may be made subject to other decision rules as warranted by empirical needs.

The statistical model for relationship classification is as follows. Consider two mutually exclusive and exhaustive hypotheses, \mathcal{R} and $\hat{\mathcal{R}}$. It holds from Bayes’ well-known theorem [108] that

$$P(\mathcal{R}|E, I) = \frac{P(E|\mathcal{R})P(\mathcal{R}|I)}{P(E)} = \frac{P(E|\mathcal{R})P(\mathcal{R}|I)}{P(E|\mathcal{R})P(\mathcal{R}|I) + P(E|\hat{\mathcal{R}})P(\hat{\mathcal{R}}|I)} \quad (\text{A1})$$

Letting $\mathcal{R}_1, \dots, \mathcal{R}_r$ denote r mutually exclusive and exhaustive hypotheses, Equation (A1) can be generalized by the *second law of probability* to obtain the following model:

$$P(\mathcal{R}_i|E_n, I) = \frac{P(E_n|\mathcal{R}_i)P(\mathcal{R}_i|I)}{\sum_{j=1}^r P(E_n|\mathcal{R}_j)P(\mathcal{R}_j|I)} \text{ for } i = 1, \dots, r, \tag{A2}$$

when $\sum_{j=1}^r P(E_n|\mathcal{R}_j)P(\mathcal{R}_j|I) \neq 0$. As can be seen from Equation (A2), two fundamental terms— $P(E|\mathcal{R})$ and $P(\mathcal{R}|I)$ —comprise the model.

By way of example, for a pair of genotypes, the posterior probability for the POP relationship will be calculated as follows:

$$Pr[H_{PO}|E, I] = \frac{\mathcal{L}_{PO} \cdot \pi_{PO}}{\mathcal{L}_{ID} \cdot \pi_{ID} + \mathcal{L}_{PO} \cdot \pi_{PO} + \mathcal{L}_{FS} \cdot \pi_{FS} + \mathcal{L}_{HS} \cdot \pi_{HS} + \mathcal{L}_{FC} \cdot \pi_{FC} + \mathcal{L}_{HFC} \cdot \pi_{HFC} + \mathcal{L}_{SC} \cdot \pi_{SC} + \mathcal{L}_{HSC} \cdot \pi_{HSC} + \mathcal{L}_{NR} \cdot \pi_{NR}} \tag{A3}$$

and compared to the posterior probabilities of the other relationships.

In Appendix B, I begin with the first term, describing the conditional single-locus and cumulative likelihood functions.

Appendix B. Single-Locus and Cumulative Likelihoods

The model structure is extendable to other genetic systems (e.g., haplodiploidy) and inheritance patterns (dominant, sex-linked, including Y-chromosome and mtDNA haplotypes). However, the study organism here is assumed to be diploid and genetic markers are assumed to be autosomal, codominant, unaffected by transmission bias, and unlinked; VNTRs (i.e., microsatellites) and/or SNPs (single-nucleotide polymorphisms) would be the markers of choice, with microsatellites utilized in the current study. Single-locus genotypes G for pairs involving individuals X and Y , respectively, comprise the evidence. For the four genes carried by X and Y at a given locus, there exists a set $\{D_i, \text{ for } i = 1, 2, \dots, 15\}$ of mutually exclusive and exhaustive identical-by-descent, IBD, modes. When distinctions between paternal and maternal genes are neglected, the set condenses to the nine modes shown in Figure A1.

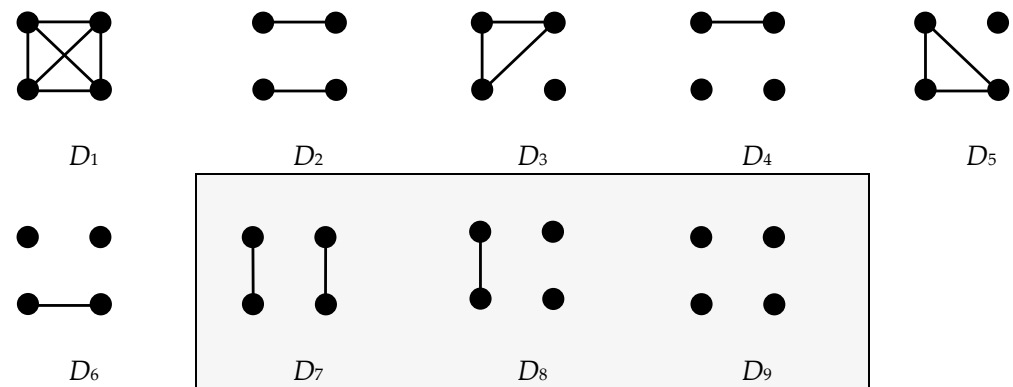


Figure A1. Nine condensed identity-by-descent modes of four genes at one locus for two diploid individuals, X and Y . By convention, the upper pair of closed circles represents the two genes from X and the lower pair represents those from Y . Connecting lines indicate genes that are IBD.

For a given relationship, let the Cotterman coefficients $k_0, k_1,$ and k_2 represent the probabilities of sharing zero, one, or two IBD genes, corresponding to descent modes $D_9, D_8,$ and $D_7,$ respectively [109]. Notation-wise, let the subscript in k_n represent 0, 1, or 2 shared IBD genes, respectively. Cotterman coefficients for the nine \mathcal{R} of interest are listed in Table A1.

Table A1. Relationship-specific values for Cotterman coefficients.

Relationship Type, \mathcal{R}	Abbreviation	k_0	k_1	k_2
Parent–offspring	<i>PO</i>	0	1	0
Monozygotic twin/identity	<i>ID</i>	0	0	1
Full sibling	<i>FS</i>	1/4	1/2	1/4
Half sibling/grand/avuncular	<i>HS+</i>	1/2	1/2	0
First cousin	<i>FC</i>	3/4	1/4	0
Half-first cousin	<i>HFC</i>	7/8	1/8	0
Second cousin	<i>SC</i>	15/16	1/16	0
Half-second cousin	<i>HSC</i>	31/32	1/32	0
Unrelated	<i>UR</i>	1	0	0

As is discussed in the main text, half relations—half siblings, half-first cousins, and half-second cousins—are expected to occur more frequently than full relations in many marine fish populations and so are included here. However, any ‘nominal’ relationship of interest can be quantified in terms of Cotterman coefficients, fully generalizing the approach. Simulation of this process has shown that it would be generally best to include the nine relationship categories identified above for the current application and others involving close-kin classifications in natural populations (M. Tringali, *unpublished data*). However, when IDPs represent the exclusive classification target, there is no observable loss of performance in more economical $|s|$ ensembles, including that using only UR as an alternate relationship in the null.

For a sampled population, let $p_i, p_j, p_k,$ and p_l represent the reference allele frequencies corresponding to the mutually exclusive alleles $A_i, A_j, A_k,$ and A_l . At a single locus, two or more alleles are said to identical-by-state (IBS) if they exhibit the same marker phenotype. Alleles that are IBD are assumed to be IBS, barring recent mutation; however, the converse is not necessarily true. For each of the nine condensed IBD modes, there is a corresponding set of IBS modes $\{\mathcal{S}_i, \text{ for } i = 1, 2, \dots, 9\}$. Because they are not phased, redundancy in genotype probabilities of modes 3 and 5 and 4 and 6, respectively, permits the nine modes to be further reduced (collapsed) into seven. Rudimentary formulae for joint genotype probabilities for collapsed IBS modes, defining $P(\mathcal{S}_i) \equiv P((G_X, G_Y)_{\mathcal{S}_i})$, are given in Table A2.

Computationally, single-locus likelihood formulae are obtained for $\{\mathcal{R}_i\}$ given \mathcal{S}_i from the product of matrix $[\mathcal{R}_i \times k_n]^T$ represented by the last three columns in Table A1 and matrix $[P(\mathcal{S}_i) \times k_n]$ represented in Table A2.

Table A2. Generalized joint genotype probabilities for the seven fully collapsed IBS modes.

G_X	G_Y	IBS Mode	$[P(\mathcal{S}_i) \times k_n]$		
			k_0	k_1	k_2
$A_i A_i$	$A_i A_i$	\mathcal{S}_1	$P(A_i, A_i, A_i, A_i)$	$P(A_i, A_i, A_i)$	$P(A_i, A_i)$
$A_i A_i$	$A_j A_j$	\mathcal{S}_2	$P(A_i, A_i, A_j, A_j)$	-	-
$A_i A_i$	$A_i A_j$	$\mathcal{S}_{3,5}$	$2P(A_i, A_i, A_i, A_j)$	$P(A_i, A_i, A_j)$	-
$A_i A_i$	$A_j A_k$	$\mathcal{S}_{4,6}$	$2P(A_i, A_i, A_j, A_k)$	-	-
$A_i A_j$	$A_i A_j$	\mathcal{S}_7	$4P(A_i, A_i, A_j, A_j)$	$(P(A_i, A_i, A_j) + P(A_i, A_j, A_j))$	$2P(A_i, A_j)$
$A_i A_j$	$A_i A_k$	\mathcal{S}_8	$4P(A_i, A_i, A_j, A_k)$	$P(A_i, A_j, A_k)$	-
$A_i A_j$	$A_k A_l$	\mathcal{S}_9	$4P(A_i, A_j, A_k, A_l)$	-	-

That is, after transposing $[\mathcal{R}_i \times \mathbb{k}_n]^T$, formulae are generated by evaluating the following product matrix and applying the *third law of probability for dependent events*:

$$l_{\mathcal{R}} = \begin{bmatrix} P(\mathcal{S}_1)_{\mathbb{k}_0} & \cdots & P(\mathcal{S}_1)_{\mathbb{k}_2} \\ \vdots & \ddots & \vdots \\ P(\mathcal{S}_9)_{\mathbb{k}_0} & \cdots & P(\mathcal{S}_9)_{\mathbb{k}_2} \end{bmatrix} \times \begin{bmatrix} \mathbb{k}_{0\mathcal{R}_1} & \cdots & \mathbb{k}_{0\mathcal{R}_r} \\ \vdots & \ddots & \vdots \\ \mathbb{k}_{2\mathcal{R}_1} & \cdots & \mathbb{k}_{2\mathcal{R}_r} \end{bmatrix} \tag{A4}$$

as shown in Table A3.

Table A3. IBS probabilities for the seven fully collapsed modes.

Mode	IBS Probability
\mathcal{S}_1	$\mathbb{k}_0 p_i^4 + \mathbb{k}_1 p_i^3 + \mathbb{k}_2 p_i^2$
\mathcal{S}_2	$\mathbb{k}_0 p_i^2 p_j^2$
$\mathcal{S}_{3,5}$	$2\mathbb{k}_0 p_i^3 p_j + \mathbb{k}_1 p_i^2 p_j$
$\mathcal{S}_{4,6}$	$2\mathbb{k}_0 p_i^2 p_j p_k$
\mathcal{S}_7	$4\mathbb{k}_0 p_i^2 p_j^2 + \mathbb{k}_1 p_i p_j (p_i + p_j) + 2\mathbb{k}_2 p_i p_j$
\mathcal{S}_8	$4\mathbb{k}_0 p_i^2 p_j p_k + \mathbb{k}_1 p_i p_j p_k$
\mathcal{S}_9	$4\mathbb{k}_0 p_i p_j p_k p_l$

Thus, the probability of the observed genotypes for a given \mathcal{R} describes the single-locus likelihood $l_{\mathcal{R}}$ of the hypothesized relationship; that is,

$$l_{\mathcal{R}} = P(\mathcal{S}_i | \mathcal{R}) \tag{A5}$$

Because single-locus likelihoods are probabilities, the *multiplicative rule* can be applied over multiple, unlinked loci to obtain the likelihood $\mathcal{L}_{\mathcal{R}}$ of the cumulative genetic evidence for a given hypothetical relationship. For m loci,

$$P[\mathbb{E} | \mathcal{R}] \equiv \mathcal{L}_{\mathcal{R}} = \prod_{i=1}^m l_{\mathcal{R},i} \tag{A6}$$

Equations (A5) and (A6) show that the strength of the genetic evidence \mathbb{E} will be influenced by the amount and partitioning of allele polymorphism at each locus and the number of loci assayed. Therefore, when discussing \mathbb{E} -related matters, values for both m and the average number of alleles (n_a) per m should be reported. Missing data should be tallied on a per locus basis, as this information will be useful if the process is simulated (*see below*). By setting $l_{\mathcal{R},i} = 1$ in these cases, one or both missing genotypes at a given locus present no difficulty beyond their failure to inform $\mathcal{L}_{\mathcal{R}}$. It is further noted that $\mathcal{L}_{\mathcal{R}}$ values of zero and thus ‘exclusions’ are possible for \mathcal{R}_{PO} and \mathcal{R}_{ID} , but not for the other relationships. Exclusions of these two relationships can be valid analytically or non-valid when they result from mistyping.

Appendix C. Estimating Sampling Probabilities for Use as Mixing Weights

To satisfy Equation (A2), the term $P(\mathcal{R} | I)$ must be parameterized over modeled relationships. Let $\{\mathcal{F}_{\mathcal{R}}\}$ be defined as the proportional distribution of plausible relationships in a population or sample pool whose support is $\mathcal{F}_{\mathcal{R}_1}, \dots, \mathcal{F}_{\mathcal{R}_r}$, where $\psi_{\mathcal{R}_i} > 0$ and $\sum_{i=1}^r \mathcal{F}_{\mathcal{R}_i} = 1$. Without further treatment of priors, the analysis described thus far conforms to a fully Bayesian approach. When an investigator has explicit knowledge \mathcal{F} of the pair-specific propensities for a given set of relationships, this knowledge can be specified as relationship-specific priors $P(\mathcal{R}_i | I)$. In the absence of explicit priors, naïve priors (alternatively referred to as ‘uniform’ priors) can be specified, taking the form $\overline{\mathcal{F}}_{\mathcal{R}_i} \equiv (1/r)$, although this rather defeats the purpose of empirical conditioning. When values of $P(\mathcal{R}_i | I)$ are not known and mixing weights are desired for model evaluation, $\{\mathcal{F}_{\mathcal{R}}\}$ can be estimated through its latent variables $\mathcal{F}_{\mathcal{R}_i}$ from the dataset itself. That is, when a sufficient number of dyads (i.e., pairwise comparisons,

n_D) from a population or sample pool are being evaluated and when specimens were sampled under like conditions, priors can be optimized through an iterative process that estimates the sampling probability distribution ($\mathcal{J}_{\mathcal{R}}$) for each plausible relationship from the overall data. In this case, the analysis becomes an empirical Bayes approach.

There are many process-based methods for latent variable estimation and model updating, varying in computational efficiency and reliability. Kucukelbir and Blei [110] provide a cogent summary of useful methods. In the current context, computational efficiency may be a general concern. Fortunately, genotypes from a sufficient number of $\mathbb{G}_{X,Y}$ will usually be evaluated such that $\mathbb{G}_{X,Y} \gg r$. Moreover, sampling events are likely to be exchangeable—i.e., occurring under like conditions such that $\{\mathcal{J}_{\mathcal{R}}\}$ may be considered an empirical constant. Thus, to optimize $P(\mathcal{R}_i|I)$, it is often practical to elicit $\{\mathcal{J}_{\mathcal{R}}\}$ recursively using a stochastic approximation of the prior distribution via a compound sampling model. The expectation optimization (EO) algorithm is as follows:

1. Beginning initially with any user-specified (e.g., uniform) prior and base likelihoods, posterior probabilities $P[H_{\mathcal{R}}|E, I]_t$, where the subscript t denotes an iteration counter, are evaluated for each pair in the sampled dataset for each \mathcal{R} .
2. Posterior probability masses for each \mathcal{R} from all evaluated dyads are used to inform sampling distribution expectations through normalization and proportional allocation.
 - a. For each \mathcal{R} , posterior probability mass is summed $\left(\sum_{j=1}^{n_D} P[H_{\mathcal{R}}|E, I]_{t,j}\right)$ for the dataset.
 - b. For normalization, a generalized rule of succession is adopted so that no sampling probability for a plausible relationship iterates to a zero value. That is, values within the set $\{\mathcal{J}_{\mathcal{R}_i}\}$ take the normalized form $\mathcal{J}_{\mathcal{R}_i, t+1} \equiv \frac{1}{n_D+r} \left[\left(\sum_{j=1}^{n_D} P[H_{\mathcal{R}}|E, I]_{t,j}\right) + 1\right]$.
3. The normalized values of the distribution are used to update $P[H_{\mathcal{R}}|I]_{t+1}$.
4. Applying $P[H_{\mathcal{R}}|I]_{t+1}$ in step 1, steps 1–3 are repeated until the estimated sampling distribution converges in measure, which is expected to occur reasonably quickly.

The convergence criterion is a function of the absolute value of differences between t and $t + 1$ empirical sampling probabilities, each summed over all relationships. Stopping values between 10^{-3} and 10^{-4} are recommended; a stopping value of 0.0001 was used herein. Upon convergence of the EO run, the ‘optimized’ sampling distribution, $\mathbb{I}_{\mathcal{R}}$, was transformed into a sample-wide kinship distribution by multiplication of sampling probabilities with n_D . Simulations have shown that $\mathbb{I}_{\mathcal{R}}$ is robustly estimated when moderate numbers of reasonably polymorphic microsatellite DNA loci are examined (e.g., $m \geq 15$; $n_a \geq 10$) (M. Tringali, unpublished data).

Appendix D. Bayes Classifier

The description so far has focused on the model (Equation (A2)). A Bayes classifier combines that model with a ‘decision rule’. As a starting point, it is common to choose the hypothesis found to be most probable—the maximum a posteriori, or *map*, rule. Once prior probabilities, however specified, are plugged into the (final) posterior probability expectations for each pair, one relationship, \mathcal{R}^{map} , attains a maximum a posteriori value $P^{map}(\mathcal{R}|E, \mathbb{I})$, where $P^{map}(\mathcal{R}|E, \mathbb{I}) > 1/r$. That is,

$$P^{map}(\mathcal{R}_i|E_n, \mathbb{I}) = \arg \max_{\mathcal{R}_i} P(E_n|\mathcal{R}_i) P(\mathcal{R}_i|\mathbb{I}) \tag{A7}$$

For convenience, the term $P^{map}(\mathcal{R}_i|E_n, \mathbb{I})$ is shortened to $P^{map}(\mathcal{R}_i)$. The distinction between *map* and *mle* (maximum-likelihood estimation) classifiers, where

$$P^{mle} = \arg \max_{\mathcal{R}_i} P(E_n|\mathcal{R}_i) \tag{A8}$$

is evident from the term reduction in the latter, and the reduction becomes critically important in multiple comparison testing, where values of both $P^{map}(\mathcal{R}_i)$ and P^{mle} are simply

point estimates whose credence must be interpreted on a ‘study-wise’ basis. Credence can be established by first adopting the *map* rule for classification, followed by (\neq) binarization of the contingency table and predictive marginalization (i.e., determination of positive and negative predictive values, false detection rates, and false rejection rates).

In some cases, it may be helpful to rescale the relative incidences of type I and II error—e.g., investigators may be willing to ‘trade’ an increase in false rejections for a decrease in false detections. If so, one option is to recast the *map* classifier as an infimum classifier $P^{inf}(\mathcal{R}_i)$, such that only *map* posteriors occur within a specified acceptance region $\Lambda = [\lambda, 1]$:

$$P^{inf}(\mathcal{R}_i|E_n, \mathbb{I}) = \arg \max_{\{\Lambda: \mathcal{R}_i \in \Lambda\}} P(E_n|\mathcal{R}_i) P(\mathcal{R}_i|\mathbb{I}) \leftrightarrow P(E_n|\mathcal{R}_i)P(\mathcal{R}_i|\mathbb{I}) \geq \lambda \quad (\text{A9})$$

The Bayesian genealogical approach described above was used to probabilistically infer the categorical relationships for all paired combinations of 302 individuals ($n_D = 45,451$). For convenience, $P^{inf}(\mathcal{R}_i|E_n, \mathbb{I})$ where $\lambda = 0.5$ was referred to as MAP_{50} ($MAP_{\lambda*100}$) and applied as the classification criterion.

References

- Buckworth, R.; Ovenden, J.; Broderick, D.; Macbeth, G.; McPherson, G.; Phelan, M. GENETAG: Genetic Mark-Recapture for Real-Time Harvest Rate Monitoring. Pilot Studies in Northern Australia Spanish Mackerel Fisheries. Darwin Australia: Northern Territory Government, Department of Resources. 2012. Available online: <http://hdl.handle.net/102.100.100/100224?index=1> (accessed on 1 April 2023).
- Lowerre-Barbieri, S.K.; Tringali, M.D.; Shea, C.P.; Walters Burnsed, S.; Bickford, J.; Murphy, M.; Porch, C. Assessing red drum spawning aggregations and abundance in the Eastern Gulf of Mexico: A multidisciplinary approach. *ICES J. Mar. Sci.* **2018**, *76*, 516–529. [[CrossRef](#)]
- Bravington, M.V.; Skaug, H.J.; Anderson, E.C. Close-kin mark-recapture. *Stat. Sci.* **2016**, *31*, 259–274.
- Trenkel, V.M.; Charrier, G.; Lorange, P.; Bravington, M.V. Close-kin mark-recapture abundance estimation: Practical insights and lessons learned. *ICES J. Mar. Sci.* **2022**, *79*, 413–422. [[CrossRef](#)]
- Waples, R.S.; Feutry, P. Close-kin methods to estimate census size and effective population size. *Fish Fish.* **2022**, *23*, 273–293. [[CrossRef](#)]
- Lowerre-Barbieri, S.K.; Walters Burnsed, S.L.; Bickford, J.W. Assessing reproductive behavior important to fisheries management: A case study with red drum, *Sciaenops ocellatus*. *Ecol. Appl.* **2016**, *26*, 979–995. [[CrossRef](#)] [[PubMed](#)]
- Lichtenstein, M.G.G. Die Werke von Marcgrave und Piso über die Naturgeschichte Brasiliens, erläutert aus den wieder aufgefundenen Originalzeichnungen. *Abbildungen. IV. Fische. Abh. K. Akad. Wiss. Berlin* **1822**, 1820–1821, 267–288.
- Sadovy, Y.; Eklund, A.M. Synopsis of biological information on the Nassau grouper, *Epinephelus striatus* (Bloch 1792), and the jewfish, *E. itajara* (Lichtenstein 1822). *NOAA Tech. Rep. NMFS* **1999**, *146*, 65.
- Koenig, C.C.; Coleman, F.C.; Eklund, A.M.; Schull, J.; Ueland, J. Mangroves as essential nursery habitat for goliath grouper (*Epinephelus itajara*). *Bull. Mar. Sci.* **2007**, *80*, 567–586.
- Bullock, L.H.; Murphy, M.D.; Godcharles, M.F.; Mitchell, M.E. Age, growth, and reproduction of jewfish *Epinephelus itajara* in the eastern Gulf of Mexico. *Fish. Bull.* **1992**, *90*, 243–249.
- Koenig, C.C.; Coleman, F.C. *The Recovering Goliath Grouper Population of the Southeastern US: Non-Consumptive Investigations for Stock Assessment*; MARFIN project NA10NMF4330123 final report; NOAA: Miami, FL, USA, 2013.
- Coleman, F.C.; Koenig, C.C.; Huntsman, G.R.; Musick, J.A.; Eklund, A.M.; McGovern, J.C.; Sedberry, G.R.; Chapman, R.W.; Grimes, C.B. Long-lived Reef Fishes: The Grouper-Snapper Complex. *Fisheries* **2000**, *25*, 14–21. [[CrossRef](#)]
- Stallings, C.D. Fishery-independent data reveal negative effect of human population density on Caribbean predatory fish communities. *PLoS ONE* **2009**, *4*, e1010. [[CrossRef](#)] [[PubMed](#)]
- Aguilar-Perera, A.; Gonzalez-Salas, C.; Tuz-Sulub, A.; Villegas-Hernandez, H. Fishery of the Atlantic Goliath Grouper, *Epinephelus itajara* (Teleostei: Epinephelidae) based on local ecological knowledge and fishery records in Yucatan Mexico. *Revista Biología Tropical.* **2009**, *57*, 557–566.
- McClenachan, L. Historical declines of Atlantic Goliath Grouper populations in South Florida, USA. *Endanger. Species Res.* **2009**, *7*, 175–181. [[CrossRef](#)]
- Cass-Calay, S.L.; Schmidt, T.W. Monitoring changes in the catch rates and abundance of juvenile Atlantic Goliath Grouper using the ENP creel survey, 1973–2006. *Endanger. Species Res.* **2009**, *7*, 183–193. [[CrossRef](#)]
- Bertoncini, A.A.; Aguilar-Perera, A.; Barreiros, J.; Craig, M.T.; Ferreira, B.; Koenig, C. *Epinephelus Itajara*. In *The IUCN Red List of Threatened Species*; International Union for Conservation of Nature and Natural Resources: Cambridge, UK, 2018. [[CrossRef](#)]

18. SEDAR (Southeast Data, Assessment, and Review Cooperative). SEDAR 47 Stock Assessment Report. Southeastern U. S. Goliath Grouper. 2016. Available online: <https://sedarweb.org/documents/sedar-47-final-stock-assessment-report-southeastern-u-s-goliath-grouper/> (accessed on 1 April 2023).
19. Koenig, C.C.; Coleman, F.C.; Kingon, K. Pattern of recovery of the goliath grouper *Epinephelus itajara* population in the southeastern US. *Bull. Mar. Sci.* **2011**, *87*, 891–911. [[CrossRef](#)]
20. Mann, D.A.; Locascio, J.V.; Coleman, F.C.; Koenig, C.C. Goliath grouper *Epinephelus itajara* sound production and movement patterns on aggregation sites. *Endanger. Species Res.* **2009**, *7*, 229–236. [[CrossRef](#)]
21. Ellis, R.D.; Koenig, C.C.; Coleman, F.C. Spawning-related Movement Patterns of Goliath Grouper (*Epinephelus itajara*) off the Atlantic Coast of Florida. *Proc. Gulf Carib. Res. Inst.* **2014**, *66*, 395–400.
22. Koenig, C.C.; Bueno, L.S.; Coleman, F.C.; Cusick, J.A.; Ellis, R.D.; Kingon, K.; Locascio, J.V.; Malinowski, C.; Murie, D.J.; Stallings, C.D. Diel, lunar, and seasonal spawning patterns of the Atlantic goliath grouper, *Epinephelus itajara*, off Florida, United States. *Bull. Mar. Sci.* **2017**, *93*, 391–406. [[CrossRef](#)]
23. Bullock, L.H.; Smith, G.B. Seabasses (Pisces: Serranidae). In *Memoirs of the Hourglass Cruises*; Florida Marine Research Institute Department of Natural Resources: St. Petersburg, FL, USA, 1991.
24. Lara, M.R.; Schull, J.; Jones, D.L.; Allman, R. Early life history stages of Atlantic Goliath Grouper *Epinephelus itajara* (Pisces: Epinephelidae) from Ten Thousand Islands, Florida. *Endanger. Species Res.* **2009**, *7*, 221–228. [[CrossRef](#)]
25. Waples, R.S.; Do, C.; Choquet, J. Calculating N_e and N_e/N in age-structured populations: A hybrid Felsenstein–Hill approach. *Ecology* **2011**, *92*, 1513–1522. [[CrossRef](#)]
26. Murata, R.; Nozu, R.; Mushirobira, Y.; Amagai, T.; Fushimi, J.; Kobayashi, Y.; Soyano, K.; Nagahama, Y.; Nakamura, M. Testicular inducing steroidogenic cells trigger sex change in groupers. *Sci. Rep.* **2021**, *11*, 11117. [[CrossRef](#)]
27. Palma, P.; Nocillado, J.; Superio, J.; de Jesus Ayson, E.G.; Ayson, F.; Bar, I.; Elizur, A. Gonadal response of juvenile protogynous grouper (*Epinephelus fuscoguttatus*) to long-term recombinant follicle-stimulating hormone administration. *Biol. Reprod.* **2019**, *100*, 798–809. [[CrossRef](#)] [[PubMed](#)]
28. Clutton-Brock, T. *Reproductive Success*, 3rd ed.; University of Chicago Press: Chicago, IL, USA, 1988.
29. Hill, W.G. Effective size of population with overlapping generations. *Theoretical Pop. Biol.* **1972**, *3*, 278–289. [[CrossRef](#)] [[PubMed](#)]
30. Johnson, D.L. Inbreeding in populations with overlapping generations. *Genetics* **1977**, *87*, 581–591. [[CrossRef](#)]
31. Crow, J.F.; Denniston, C. Inbreeding and variance effective population numbers. *Evolution* **1988**, *42*, 82–95. [[CrossRef](#)]
32. Wang, J. A new method for estimating effective population sizes from a single sample of multilocus genotypes. *Mol. Ecol.* **2009**, *18*, 2148–2164. [[CrossRef](#)]
33. Hill, W.G. A note on effective population size with overlapping generations. *Genetics* **1979**, *92*, 317–322. [[CrossRef](#)] [[PubMed](#)]
34. Felsenstein, J. Inbreeding and variance effective numbers in populations with overlapping generations. *Genetics* **1971**, *68*, 581–597. [[CrossRef](#)]
35. Leslie, P.H. The use of matrices in certain population mathematics. *Biometrika* **1945**, *33*, 183–212. [[CrossRef](#)]
36. Waples, R.S.; England, P.R. Estimating Contemporary Effective Population Size on the Basis of Linkage Disequilibrium in the Face of Migration. *Genetics* **2011**, *189*, 633–644. [[CrossRef](#)]
37. Ryman, N.; Laikre, L.; Hössjer, O. Do estimates of contemporary effective population size tell us what we want to know? *Mol. Ecol.* **2019**, *28*, 1904–1918. [[CrossRef](#)] [[PubMed](#)]
38. Waples, R.S. Life-history traits and effective population size in species with overlapping generations revisited: The importance of adult mortality. *Heredity* **2016**, *117*, 241–250. [[CrossRef](#)] [[PubMed](#)]
39. Simmonds, J.; MacLennan, D. *Fisheries Acoustics: Theory and Practice*; Blackwell Publishing Ltd: Hoboken, NJ, USA, 2005.
40. Pine, W.E.; Hightower, J.E.; Coggins, L.G.; Lauretta, M.V.; Pollock, K.H. Design and analysis of tagging studies. In *Fisheries Techniques*, 3rd ed.; Zale, A.V., Parrish, D.L., Sutton, T.M., Eds.; American Fisheries Society: Bethesda, MD, USA, 2012; pp. 521–572.
41. Murie, D.J.; Parkyn, D.C.; Koenig, C.C.; Coleman, F.C.; Schull, J.; Frias-Torres, S. Evaluation of fin-rays as a nonlethal ageing method for protected goliath grouper *Epinephelus itajara*. *Endanger. Species Res.* **2009**, *7*, 213–220. [[CrossRef](#)]
42. Do, C.; Waples, R.S.; Peel, D.; Macbeth, G.M.; Tillett, B.J.; Ovenden, J.R. NeEstimator v2: Re-implementation of software for the estimation of contemporary effective population size (N_e) from genetic data. *Mol. Ecol. Res.* **2014**, *14*, 209–214. [[CrossRef](#)] [[PubMed](#)]
43. Hill, W.G. Estimation of effective population size from data on linkage disequilibrium. *Genet. Res.* **1981**, *38*, 209–216. [[CrossRef](#)]
44. Waples, R.S.; Do, C. Linkage disequilibrium estimates of contemporary N_e using SNPs and highly polymorphic molecular markers: An evaluation of precision and bias. *Evol. Appl.* **2010**, *3*, 244–262. [[CrossRef](#)]
45. Waples, R.S. A bias correction for estimates of effective population size based on linkage disequilibrium at unlinked gene loci. *Conserv. Genet.* **2006**, *7*, 167–184. [[CrossRef](#)]
46. Jones, A.; Ovenden, J.; Wang, Y.G. Improved confidence intervals for the linkage disequilibrium method for estimating effective population size. *Heredity* **2016**, *117*, 217–223. [[CrossRef](#)]
47. Waples, R.K.; Larson, W.A.; Waples, R.S. Estimating contemporary effective population size in non-model species using linkage disequilibrium across thousands of loci. *Heredity* **2016**, *117*, 233–240. [[CrossRef](#)]

48. Waples, R.S.; Antao, T.; Luikart, G. Effects of overlapping generations on linkage disequilibrium estimates of effective population size. *Genetics* **2014**, *197*, 769–780. [[CrossRef](#)]
49. Waples, R.S. Tiny estimates of the N_e/N ratio in marine fishes: Are they real? *J. Fish Biol.* **2016**, *89*, 2479–2504. [[CrossRef](#)]
50. Then, A.Y.; Hoenig, J.M.; Hall, N.G.; Hewitt, D.A. Evaluating the predictive performance of empirical estimators of natural mortality rate using information on over 200 fish species. *ICES J. Mar. Sci.* **2015**, *72*, 82–92. [[CrossRef](#)]
51. Wang, J. Individual identification from genetic marker data: Developments and accuracy comparisons of methods. *Mol. Ecol. Resour.* **2016**, *16*, 163–175. [[CrossRef](#)]
52. Rochet, M.J. Effects of fishing on the population. In *Fish Reproductive Biology*; Jakobsen, T., Fogarty, M.J., Megrey, B.A., Moksness, E., Eds.; Wiley-Blackwell Scientific Publications: Chichester, UK, 2009; pp. 172–206.
53. Marty, L.; Rochet, M.J.; Ernande, B. Temporal trends in age and size at maturation of four North Sea gadid species: Cod, haddock, whiting and Norway pout. *Mar. Ecol. Prog. Ser.* **2014**, *497*, 179–197. [[CrossRef](#)]
54. Hunter, A.; Speirs, D.C.; Heath, M.R. Fishery-induced changes to age and length dependent maturation schedules of three demersal fish species in the Firth of Clyde. *Fish. Res.* **2015**, *170*, 14–23. [[CrossRef](#)]
55. Waite, T.A.; Parker, P.G. Dimensionless Life Histories and Effective Population Size. *Conserv. Biol.* **1996**, *10*, 1456–1462. Available online: <http://www.jstor.org/stable/2386920> (accessed on 1 April 2023). [[CrossRef](#)]
56. Rose, K.A.; Cowan, J.H.; Winemiller, K.O., Jr.; Myers, R.A.; Hilborn, R. Compensatory density dependence in fish populations: Importance, controversy, understanding and prognosis. *Fish Fish.* **2001**, *2*, 293–327. [[CrossRef](#)]
57. Devlin, R.H.; Nagahama, Y. Sex determination and sex differentiation in fish: An overview of genetic, physiological, and environmental influences. *Aquaculture* **2002**, *208*, 191–364. [[CrossRef](#)]
58. Heppell, S.S.; Heppell, S.A.; Coleman, F.C.; Koenig, C.C. Models to compare management options for a protogynous fish. *Ecol. Appl.* **2006**, *16*, 238–249. [[CrossRef](#)]
59. Brooks, E.N.; Shertzer, K.W.; Gedamke, T.; Vaughan, D.S. Stock assessment of protogynous fish: Evaluating measures of spawning biomass used to estimate biological reference points. *Fish. Bull.* **2008**, *106*, 12–23.
60. Ellis, R.D.; Powers, J.E. Gag grouper, marine reserves, and density-dependent sex change in the Gulf of Mexico. *Fish. Res.* **2012**, *115*, 89–98. [[CrossRef](#)]
61. Lowerre-Barbieri, S.; Menendez, H.; Bickford, J.; Switzer, T.S.; Barbieri, L.; Koenig, C. Testing assumptions about sex change and spatial management in the protogynous gag grouper, *Mycteroperca microlepis*. *Mar. Ecol. Prog. Ser.* **2020**, *639*, 199–214. [[CrossRef](#)]
62. Taylor, R.G.; Whittington, J.A.; Grier, H.J.; Crabtree, R.E. Age, growth, maturation, and protandric sex reversal in common snook, *Centropomus undecimalis*, from the east and west coasts of South Florida. *Fish. Bull.* **2000**, *98*, 612–624.
63. Waples, R.S.; Reed, T.E. Null models for the Opportunity for Selection. *Am. Nat.* **2023**, *201*. [[CrossRef](#)]
64. Soloviev, A.; Hirons, A.; Maingot, C.; Whitney Dean, C.; Dodge, R.E.; Yankovsky, A.E.; Wood, J.; Weisberg, R.H.; Luther, M.E.; McCreary, J.P. Southward Flow on the Western Flank of the Florida Current. Deep Sea Research Part I: Oceanographic Research Papers. 2017, pp. 94–105. Available online: https://nsuworks.nova.edu/occ_facarticles/826 (accessed on 1 April 2023).
65. Leshner, A.T. An Analysis of Larval Dispersal and Retention within the South Atlantic Bight Using Satellite-Tracked Drifters Released on Reef Fish Spawning Grounds. Master's Thesis, College of Charleston, Charleston, SC, USA, 2008.
66. Lee, A.M.; Engen, S.; Sæther, B.-E. The influence of persistent individual differences and age at maturity on effective population size. *Proc. R. Soc. B Biol. Sci.* **2011**, *278*, 3303–3312. [[CrossRef](#)] [[PubMed](#)]
67. Weber, D.N.; Fields, A.T.; Patterson III, W.F.; Barnett, B.K.; Hollenbeck, C.M.; Portnoy, D.S. Novel epigenetic age estimation in wild-caught Gulf of Mexico reef fishes. *Can. J. Fish. Aquat. Sci.* **2021**, *79*, 1–5. [[CrossRef](#)]
68. Waples, R.S.; Grewe, P.M.; Bravington, M.W.; Hillary, R.; Feutry, P. Robust estimates of a high N_e/N ratio in a top marine predator, southern bluefin tuna. *Sci. Adv.* **2018**, *4*, eaar7759. [[CrossRef](#)]
69. Marshall, C.T.; Needle, C.L.; Thorsen, A.; Kjesbu, O.S.; Yaragina, N.A. Systematic bias in estimates of reproductive potential of an Atlantic cod (*Gadus morhua*) stock: Implications for stock-recruit theory and management. *Can. J. Fish. Aquat. Sci.* **2006**, *63*, 980–994. [[CrossRef](#)]
70. Barneche, D.R.; Ross Robertson, D.; White, C.R.; Marshall, D.J. Fish reproductive-energy output increases disproportionately with body size. *Science* **2018**, *360*, 642–645. [[CrossRef](#)]
71. Nunney, L. The influence of variation in female fecundity on effective population size. *Biol. J. Linn. Soc.* **1996**, *59*, 411–425. [[CrossRef](#)]
72. Lee, A.M.; Myhre, A.M.; Markussen, S.S.; Engen, S.; Solberg, E.J.; Haanes, H.; Røed, K.; Herfindal, I.; Heim, M.; Sæther, B.-E. Decomposing demographic contributions to the effective population size with moose as a case study. *Mol. Ecol.* **2020**, *29*, 56–70. [[CrossRef](#)] [[PubMed](#)]
73. Wen, Z.; Pollock, K.H.; Nichols, J.D.; Waser, P.M.; Cao, W. Using imputation and mixture model approaches to integrate multi-state capture-recapture models with assignment information. *Biometrics* **2014**, *70*, 323–334. [[CrossRef](#)] [[PubMed](#)]
74. Boys, R.M.; Oliveira, C.; Pérez-Jorge, S.; Prieto, R.; Steiner, L.; Silva, M.A. Multi-state open robust design applied to opportunistic data reveals dynamics of wide-ranging taxa: The sperm whale case. *Ecosphere* **2019**, *10*, 2150–8925. [[CrossRef](#)]
75. Franklin, I.R. Evolutionary change in small populations. In *Conservation Biology: An Evolutionary–Ecological Perspective*; Soulé, M.E., Wilcox, B.A., Eds.; Sinauer Associates: Sunderland, MA, USA, 1980; pp. 135–150.

76. Kimura, M. Solution of a process of random genetic drift with a continuous model. *Proc. Nat. Acad. Sci. USA* **1955**, *41*, 144–150. [[CrossRef](#)]
77. Lynch, M.; Lande, R. Evolution and extinction in response to environmental change. In *Biotic Interactions and Global Change*; Kareiva, P.M., Kingsolver, J.G., Huey, R.B., Eds.; Sinauer Associates Inc: Sunderland, MA, USA, 1993; pp. 234–250.
78. Willi, Y.; van Buskirk, J.; Hoffmann, A.A. Limits of the adaptive potential of small populations. *Annual Review of Ecology. Evol. Syst.* **2006**, *37*, 433–458. [[CrossRef](#)]
79. Crow, J.F. Some possibilities for measuring selection intensities in man. *Human Biol.* **1958**, *30*, 1–13.
80. Arnold, S.J.; Wade, M.J. On the measurement of natural and sexual selection: Applications. *Evolution* **1984**, *38*, 720–734. [[CrossRef](#)]
81. Brodie III, E.D.; Moore, A.J.; Janzen, F.J. Visualizing and quantifying natural selection. *Trends Ecol. Evol.* **1995**, *10*, 313–318. [[CrossRef](#)]
82. Lowerre-Barbieri, S.; DeCelles, G.; Pepin, P.; Catala, I.A.; Muhling, B.; Erisman, B.; Cadrin, S.X.; Alós, J.; Ospina-Alvarez, A.; Stachura, M.M.; et al. Reproductive resilience: A paradigm shift in understanding spawner-recruit systems in exploited marine fish. *Fish Fish.* **2017**, *18*, 285–312. [[CrossRef](#)]
83. Árnason, E.; Koskela, J.; Halldórsdóttir, K.; Eldon, B. Sweepstakes reproductive success via pervasive and recurrent selective sweeps. *Elife.* **2023**, *12*, e80781. [[CrossRef](#)]
84. Williams, G.C. *Sex and Evolution*. Princeton; Princeton University Press: Princeton, NJ, USA, 1975.
85. Hedgecock, D. Does variance in reproductive success limit effective population size of marine organisms. In *Genetics and Evolution of Aquatic Organisms*; Beaumont, A., Ed.; Chapman & Hall: London, UK, 1994; pp. 122–134.
86. Hedgecock, D.; Pudovkin, A.I. Sweepstakes reproductive success in highly fecund marine fish and shellfish: A review and commentary. *Bull. Mar. Sci.* **2011**, *87*, 971–1002. [[CrossRef](#)]
87. Marteinsdottir, G.; Begg, G.A. Essential relationships incorporating the influence of age, size and condition on variables required for estimation of reproductive potential in Atlantic cod *Gadus Morhua*. *Mar. Ecol. Prog. Ser.* **2002**, *235*, 235–256. [[CrossRef](#)]
88. Ryman, N.; Laikre, L. Effects of supportive breeding on the genetically effective population size. *Conserv. Biol.* **1991**, *5*, 325–329. [[CrossRef](#)]
89. Ryman, N.; Jorde, P.E.; Laikre, L. Supportive breeding and inbreeding effective number: Reply to Nomura. *Conserv. Biol.* **1999**, *13*, 673–676. [[CrossRef](#)]
90. Tringali, M.D.; Bert, T.M. Risk to effective population size should be an important consideration in fish stock-enhancement programs. In: Proceedings of marine stock enhancement: A new perspective. *Bull. Mar. Sci.* **1998**, *62*, 641–660.
91. Waples, R.S.; Hindar, K.; Karlsson, S.; Hard, J.J. Evaluating the Ryman-Laikre effect for marine stock enhancement and aquaculture. *Curr. Zool.* **2016**, *62*, 617–627. [[CrossRef](#)] [[PubMed](#)]
92. Christie, M.R.; Marine, M.L.; Fox, S.E.; French, R.A.; Blouin, M.S. A single generation of domestication heritably alters the expression of hundreds of genes. *Nat. Commun.* **2016**, *7*, 10676. [[CrossRef](#)]
93. Kültz, D.A. *Primer of Ecological Aquaculture*; Oxford University Press: Oxford, UK, 2022; p. 304.
94. Frankham, R. Genetic rescue of small inbred populations: Meta-analysis reveals large and consistent benefits of gene flow. *Mol. Ecol.* **2015**, *24*, 2610–2618. [[CrossRef](#)]
95. Tringali, M.D. Genetic Changes in Natural Populations Caused by the Release of Cultured Fishes. 2003. Graduate Theses and Dissertations. Available online: <https://scholarcommons.usf.edu/etd/1495> (accessed on 1 April 2023).
96. Jamieson, I.G.; Allendorf, F.W. How does the 50/500 rule apply to MVPs? *Trends Ecol. Evol.* **2012**, *27*, 578–584. [[CrossRef](#)]
97. Pérez-Pereira, N.; Wang, J.; Quesada, H.; Caballero, A. Prediction of the minimum effective size of a population viable in the long term. *Biodivers. Conserv.* **2022**, *31*, 2763–2780. [[CrossRef](#)]
98. Goudet, J. Fstat (version 1.2): A computer program to calculate *f*-statistics. *J. Hered.* **1995**, *86*, 485–486. [[CrossRef](#)]
99. Lunt, D.; Hutchinson, W.; Carvalho, G. An efficient method of PCR-based isolation of microsatellite arrays (PIMA). *Mol. Ecol.* **1999**, *8*, 891–894.
100. Raymond, M.; Rousset, F. GENEPOP (version 1.2): Population genetics software for exact tests and ecumenicism. *J. Hered.* **1995**, *86*, 248–249. [[CrossRef](#)]
101. Rousset, F. Genepop'007: A complete reimplement of the GENEPOP software for Windows and Linux. *Mol. Ecol. Resour.* **2008**, *8*, 103–106. [[CrossRef](#)]
102. Seyoum, S.; Tringali, M.D.; Sullivan, J.G. Isolation and characterization of 27 polymorphic microsatellite loci for the common snook, *Centropomus undecimalis*. *Mol. Ecol. Notes.* **2005**, *5*, 922–927. [[CrossRef](#)]
103. Seyoum, S.; Tringali, M.D.; Barthel, B.L.; Puchulutegui, C.; Davis, M.C.; Collins, A.B.; Craig, M.T. Isolation and characterization of 29 polymorphic microsatellite markers for the endangered Atlantic goliath grouper (*Epinephelus itajara*), and the Pacific goliath grouper (*E. quinquefasciatus*). *Cons. Gen. Res.* **2013**, *5*, 729–732. [[CrossRef](#)]
104. Seyoum, S.; Puchulutegui, C.; McBride, R.S. Isolation and characterization of 24 polymorphic microsatellite loci for the study of genetic population structure of the sheepshead *Archosargus probatocephalus* (Actinopterygii, Perciformes, Sparidae). *BMC Res. Notes* **2016**, *9*, 251. [[CrossRef](#)] [[PubMed](#)]
105. Marshall, T.C.; Slate, J.; Kruuk, L.E.B.; Pemberton, J.M. Statistical confidence for likelihood-based paternity inference in natural populations. *Mol. Ecol.* **1998**, *7*, 639–655. [[CrossRef](#)]

106. Madigan, D.; Raftery, A.E. Model Selection and Accounting for Model Uncertainty in Graphical Models Using Occam's Window. *J. Am. Stat. Assoc.* **1994**, *89*, 1535–1546. [[CrossRef](#)]
107. Sorenson, H.W. *Parameter Estimation: Principles and Problems (v. 9)*; Marcel Dekker: New York, NY, USA, 1980.
108. Bayes, T. An Essay Towards Solving a Problem in the Doctrine of Chances. *Phil. Trans. Royal Soc.* **1763**, *53*, 370–418. [[CrossRef](#)]
109. Cotterman, C.W. A Calculus for Statistico-Genetics. Ph.D. Thesis, The Ohio State University, Columbus, OH, USA, 1940.
110. Kucukelbir, A.; Blei, D.M. Population Empirical Bayes. *arXiv* **2015**, arXiv:1411.0292.

Disclaimer/Publisher's Note: The statements, opinions and data contained in all publications are solely those of the individual author(s) and contributor(s) and not of MDPI and/or the editor(s). MDPI and/or the editor(s) disclaim responsibility for any injury to people or property resulting from any ideas, methods, instructions or products referred to in the content.